

# Journal of Visualized Experiments

## Temperature-Controlled Assembly and Characterization of a Droplet Interface Bilayer --Manuscript Draft--

Article Type:	Invited Methods Collection - JoVE Produced Video
Manuscript Number:	JoVE62362R1
Full Title:	Temperature-Controlled Assembly and Characterization of a Droplet Interface Bilayer
Corresponding Author:	Stephen Andrew Sarles UNITED STATES
Corresponding Author's Institution:	
Corresponding Author E-Mail:	ssarles@utk.edu
Order of Authors:	Jessie Ringley Stephen Andrew Sarles
Additional Information:	
Question	Response
Please specify the section of the submitted manuscript.	Bioengineering
Please indicate whether this article will be Standard Access or Open Access.	Standard Access (US\$2,400)
Please indicate the <b>city, state/province, and country</b> where this article will be <b>filmed</b> . Please do not use abbreviations.	Knoxville, TN
Please confirm that you have read and agree to the terms and conditions of the author license agreement that applies below:	I agree to the <a href="#">Author License Agreement</a>
Please provide any comments to the journal here.	Andy Sarles should be listed as co-author ORCID ID:0000-0002-6694-6451

**TITLE:**

Temperature-Controlled Assembly and Characterization of a Droplet Interface Bilayer

**AUTHOR AND AFFILIATIONS:**

Jessie D. Ringley<sup>1</sup>, Stephen A. Sarles<sup>1</sup>

<sup>1</sup>Department of Mechanical, Aerospace and Biomedical Engineering, University of Tennessee, Knoxville

Corresponding Author:

Stephen A. Sarles (ssarles@utk.edu)

Email Addresses of Co-Author:

Stephen A. Sarles (ssarles@utk.edu)

Jessie Ringley (jringle1@vols.utk.edu)

**KEYWORDS:**

engineering, bioengineering, lipid bilayer, droplet interface bilayer, feedback temperature control, capacitance measurements, ion channel, life sciences

**SUMMARY:**

This protocol details the use of a feedback temperature-controlled heating system to promote lipid monolayer assembly and droplet interface bilayer formation for lipids with elevated melting temperatures, and capacitance measurements to characterize temperature-driven changes in the membrane.

**ABSTRACT**

The droplet interface bilayer (DIB) method for assembling lipid bilayers (i.e., DIBs) between lipid-coated aqueous droplets in oil offers key benefits versus other methods: DIBs are stable and often long-lasting, bilayer area can be reversibly tuned, leaflet asymmetry is readily controlled via droplet compositions, and tissue-like networks of bilayers can be obtained by adjoining many droplets. Forming DIBs requires spontaneous assembly of lipids into high density lipid monolayers at the surfaces of the droplets. While this occurs readily at room temperature for common synthetic lipids, a sufficient monolayer or stable bilayer fails to form at similar conditions for lipids with melting points above room temperature, including some cellular lipid extracts. This behavior has likely limited the compositions—and perhaps the biological relevance—of DIBs in model membrane studies. To address this problem, an experimental protocol is presented to carefully heat the oil reservoir hosting DIB droplets and characterize the effects of temperature on the lipid membrane. Specifically, this protocol shows how to use a thermally conductive aluminum fixture and resistive heating elements controlled by a feedback loop to prescribe elevated temperatures, which improves monolayer assembly and bilayer formation for a wider set of lipid types. Structural characteristics of the membrane, as well as the thermotropic phase transitions of the lipids comprising the bilayer, are quantified by measuring the changes in electrical capacitance of the DIB. Together, this procedure can aid in evaluating

biophysical phenomena in model membranes over various temperatures, including determining an effective melting temperature ( $T_M$ ) for multi-component lipid mixtures. This capability will thus allow for closer replication of natural phase transitions in model membranes and encourage the formation and use of model membranes from a wider swath of membrane constituents, including those that better capture the heterogeneity of their cellular counterparts.

## INTRODUCTION

Cellular membranes are selectively permeable barriers comprising of up to thousands of lipid types<sup>1</sup>, proteins, carbohydrates, and sterols that encapsulate and subdivide all living cells. Understanding how their compositions affect their functions and revealing how natural and synthetic molecules interact with, adhere to, disrupt, and translocate cellular membranes are, therefore, important areas of research with wide-reaching implications in biology, medicine, chemistry, physics, and materials engineering.

These aims for discovery directly benefit from proven techniques for assembling, manipulating, and studying model membranes—including lipid bilayers assembled from synthetic or naturally occurring lipids—that mimic the composition, structure, and transport properties of their cellular counterparts. In recent years, the droplet interface bilayer (DIB) method<sup>2-4</sup> for constructing a planar lipid bilayer between lipid-coated water droplets in oil has received significant attention<sup>5-23</sup>, and has demonstrated practical advantages over other approaches for model membrane formation: the DIB method is simple to perform, requires no sophisticated fabrication or preparation (e.g., “painting”) of a substrate to support the membrane, consistently yields membranes with superior longevity, allows for standard electrophysiology measurements, and simplifies the formation of model membranes with asymmetric leaflet compositions<sup>3</sup>. Because the bilayer forms spontaneously between droplets and each droplet can be tailored in position and makeup, the DIB technique has also attracted considerable interest in developing cell-inspired material systems that build on the use of stimuli-responsive membranes<sup>18,24-29</sup>, balanced compartmentalization and transport<sup>14,30,31</sup>, and tissue-like materials<sup>17,23,32-36</sup>.

The majority of published experiments on model membranes, including those with DIBs, have been performed at room temperature (RT, ~20-25 °C) and with a handful of synthetic lipids (e.g., DOPC, DPhPC, etc.). This practice limits the scope of biophysical questions that can be studied in model membranes and based on observation, it can also restrict the types of lipids that can be used to assemble DIBs. For example, synthetic lipids such as DPPC, which has a melting temperature of 42 °C, does not assemble tightly-packed monolayers or form DIBs at RT<sup>37</sup>. DIB formation at room temperature has also proven difficult for natural extracts, such as those from mammals (e.g., brain total lipid extract, BTLE)<sup>38</sup> or bacteria (e.g., *Escherichia coli* total lipid extract, ETLE)<sup>37</sup>, which contain many different types of lipids and originate from cells that reside at elevated temperatures (37 °C). Enabling study of diverse compositions thus provides opportunities to understand membrane-mediated processes in biologically relevant conditions.

Raising the temperature of the oil can serve two purposes: it increases the kinetics of monolayer assembly and it can cause lipids to undergo a melting transition to reach a liquid disordered phase. Both consequences aid in monolayer assembly<sup>39</sup>, a pre-requisite for a DIB. In addition to

heating for bilayer formation, cooling the membrane after the formation can be used to identify thermotropic transitions in single lipid bilayers<sup>38</sup>, including those in natural lipid mixtures (e.g., BTLE) that can be difficult to detect using calorimetry. Aside from assessing thermotropic transitions of lipids, precisely varying the temperature of the DIB can be used to study temperature-induced changes in membrane structure<sup>38</sup> and examine how lipid composition and fluidity affect the kinetics of membrane-active species (e.g., pore-forming peptides and transmembrane proteins<sup>37</sup>), including in mammalian and bacterial model membranes and at a physiological temperature (37 °C).

Herein, a description of how to assemble a modified DIB oil reservoir and operate feedback-temperature control to enable monolayer assembly and bilayer formation at temperatures higher than RT will be explained. Distinguished from a previous protocol<sup>40,41</sup>, explicit detail is included regarding the integration of instrumentation needed for measuring and controlling temperature in parallel to assembly and characterization of the DIB in the oil reservoir. The procedure will thus enable a user to apply this method for forming and studying DIBs across a range of temperatures in a variety of scientific contexts. Moreover, the representative results provide specific examples for the types of measurable changes in both membrane structure and ion transport that can occur as temperature is varied. These techniques are important additions to the many biophysical studies that can be designed and performed effectively in DIBs, including studying the kinetics of membrane-active species in different membrane compositions.

## PROTOCOL:

### 1. Heated fixture preparation

1.1. Gather 2 pieces of 1 mm thick insulative rubber trimmed to 25 mm x 40 mm in length, 2 pieces of a 6 mm-thick rubber that are also 25 mm x 40 mm, a prepared aluminum base fixture assembly, and an acrylic oil reservoir that fits in the viewing window of the aluminum base fixture (see **Figures S1, S2, and S3** for details on fabrication and an exploded view of assembly). Prepare the aluminum fixture first by attaching to the bottom of the fixture a glass coverslip viewing window with UV curable adhesive and adhering 1 resistive heating element to the top of each 25 mm x 25 mm side flange of the fixture.

1.2. Place the thinner rubber pieces onto the stage of the microscope such that the long edge of each piece is tangential to the stage opening as shown in (**Figure 1**).

1.3. Position the aluminum-base fixture on top of the insulative pads with the viewing window of the fixture centered above the objective lens. Proper alignment is required for imaging the connected droplets.

1.4. Place a thicker piece of rubber on top of each resistive heating element and use a microscope stage clip to hold it in place. These pieces protect the heating elements from damage caused by the stage clips and insulate against accidental electrical shorting between the heating elements and both the aluminum fixture and the microscope stage.

133  
134 1.5. Carefully bend the measurement-end of a thermocouple to achieve a 90° angle at ~4 mm  
135 from the end.

136  
137 1.6. Insert the bent tip of the thermocouple into the lower left corner of the aluminum fixture  
138 and gently secure it with the locking screw.

139  
140 1.7. Place the acrylic reservoir into the well of the aluminum fixture. This is done prior to  
141 adding hexadecane oil to the well (step 1.8) of the aluminum fixture to minimize the risk of  
142 trapping air bubbles between the viewing window and the bottom of the acrylic reservoir, which  
143 can obstruct the view of the droplets.

144  
145 NOTE: Oil added to the viewing compartment of the aluminum fixture is used to match the  
146 refractive indices of the acrylic and glass for clearer imaging of the droplets contained within the  
147 acrylic reservoir. Thus, it is worth noting that oil in the well of the aluminum fixture does not  
148 contact the contents of the acrylic reservoir and rigorous cleaning of the aluminum fixture is not  
149 required.

150  
151 1.8. Dispense ~1,000 µL of hexadecane oil into the well of aluminum fixture (i.e., between the  
152 walls of the acrylic reservoir and aluminum fixture), taking care to not overfill. The oil level in the  
153 well of the aluminum fixture should be as high as allowable to provide a maximal surface area  
154 for heat transfer to occur, while not allowing oil to spill over the edges of the fixture onto the  
155 microscope stage or objective lens.

156  
157 1.9. Dispense ~1,000 µL of hexadecane oil into the acrylic reservoir, while remaining mindful  
158 to not overfill.

159  
160 NOTE: The acrylic reservoir should always be thoroughly cleaned between experiments. The user  
161 must employ a regiment consisting of successive rinses with ethyl-alcohol, deionized water, and  
162 dried in desiccator bowl for over 12 h, between experiments.

163  
164 **(Place figure 1 here)**

## 165 166 **2. Instrumentation for simultaneous feedback temperature control and electrical** 167 **characterization of a DIB**

168  
169 NOTE: This protocol integrates the following instruments for enabling feedback temperature  
170 control and simultaneous electrical characterization of a DIB: a personal computer (PC) with two  
171 available USB connections, patch clamp amplifier paired to a dedicated data acquisition (DAQ-1)  
172 system, a waveform generator, a second programable DAQ (DAQ-2) with voltage output and  
173 temperature input modules, and a power supply/amplifier. The following steps describe the  
174 necessary connections of these instruments (as illustrated in **Figure 2a**) needed for isolating the  
175 measurement and control of temperature from simultaneous electrophysiology of a DIB.  
176 Substitutions for equivalent instruments may be made as required.

2.1. Establish output and input connections to the DAQ-2 modules.

2.1.1. Select two pairs of screw terminals on the voltage output module for differential voltage connections and attach wire leads to these locations. Odd number terminals are common ground connections, and the even number terminals are ungrounded outputs, as shown in **(Figure 2c)**. Connect each of these two pairs of lead wires to separate screw-terminal-BNC adapters and then connect each adapter to a separate BNC cable used to route voltage signals to other instruments.

NOTE: In this setup, differential connections at terminals 0 and 1 are assigned for the temperature control output to the power amplifier, while another pair of connections at terminals 6 and 7 are designated for voltage output to be sent to the droplets via the patch clamp amplifier.

2.1.2. Referring to **(Figure 2c)**, select one set of thermocouple terminals (e.g., terminals 2 and 3 are designated as the TC1 pair) on the thermocouple input module and connect to it the thermocouple wires.

**(Place Figure 2 here)**

2.1.3. After electrical connections to the DAQ-2 modules have been made, connect the DAQ-2 chassis to a personal computer (PC) via a universal serial bus (USB) connection and connect to an electrical power source. Then confirm successful driver and software installation prior to use with a commercial software (e.g., LabVIEW).

2.2. Configure and connect a power amplifier between DAQ-2 and resistive heating elements.

2.2.1. Configure the amplifier to operate in fixed-gain amplification mode with a gain of 10X.

2.2.2. Using a banana jack-BNC adapter, connect the BNC cable originating from terminals 0 and 1 on the voltage output module **(Figure 2b)** to the input connections on the power amplifier.

2.2.3. Using additional BNC adapters and cabling, connect the output terminals of the power amplifier to both sets of heating elements, which are wired in parallel to one another and the amplifier to ensure that both elements maintain the same voltage drop during use.

2.3. Establish necessary connections for the electrophysiology equipment.

2.3.1. Connect a BNC cable originating from terminals 6 and 7 on the voltage output module **(Figure 2b)** to the Rear Switched External Command BNC connectors on the rear of the patch clamp amplifier.

2.3.2. Connect a second BNC cable between the output of waveform generator and the Front Switch External Command connection on the rear of the patch clamp amplifier.

NOTE: These two connections provide alternative methods for generating voltage waveforms that are applied to the droplet electrodes via the patch clamp amplifier. The waveform generator is especially useful for generating triangular waveform voltages used to measure membrane capacitance. The user may decide which, if either, are necessary for their own application.

2.3.3. With a third BNC cable, connect the output of the measured current located on the front panel of the patch clamp amplifier to an available analog input BNC connector on the front of DAQ-1.

2.3.4. With a fourth BNC cable, connect the output of measured membrane voltage (on the rear of the patch clamp amplifier) to a separate analog input connector on DAQ-1. This enables digitization of the voltage applied across the electrodes.

2.3.5. With the two droplet electrodes prepared and supported on micromanipulators as described in Steps 7-9 in ref.<sup>40</sup>, connect the electrode leads to the patch clamp headstage, which is attached via cable to the patch clamp amplifier.

NOTE: The role of the headstage is to control the voltage between the electrodes and measure the resulting current, which is converted into a proportional voltage that gets output by the patch clamp amplifier to DAQ-1.

2.3.6. Connect DAQ-1 to a PC via a USB connection and connect the corresponding power supply cables to both the patch clamp amplifier and DAQ-1.

2.4. Power on all measurement equipment.

NOTE: Perhaps the most important detail in this setup is to ensure the power amplifier output (mA-A) connections are electrically isolated from the headstage unit of the patch clamp amplifier, which uses a sensitive circuit to measure pA-nA level currents in a DIB.

### **3. Feedback temperature control of droplet interface bilayers**

NOTE: The following steps for operating the feedback temperature control system are based on a custom GUI created for implementing proportional-integral (PI) feedback temperature control<sup>40,42</sup> (see **Supplementary Coding Files**). Other software and control algorithms may be used instead. A copy of this program is provided to the reader with the supplementary information for the paper, however the user is responsible to configure it for their own equipment and needs.

3.1. Start the DAQ-2 software on the PC and open the temperature control program file. Once the GUI opens, open the program again by clicking on the folder icon in the bottom left corner of the GUI and selecting the temperature control program (**Figure 3**).

3.2. Enter appropriate numerical values for the proportional control gain ( $K_p$ ) and integral control gain ( $K_I$ ).

NOTE:  $K_p$  and  $K_I$  values of 0.598 and 0.00445, respectively, were found to work well in the setup. These values were determined iteratively through simulation using a system model that incorporates parameters obtained from measured open-loop heating responses (see **Figure 4**). During *open-loop heating*, the prescribed heating power is independent of the measured temperature. In contrast, *closed-loop heating* consists of continually adjusting the applied power to the heaters in a manner that helps drive the measured temperature closer to the desired temperature. This is achieved herein using a proportional-integral (PI) control scheme.

3.3. To test temperature control scheme, enter a desired set point temperature (above room temperature) and then turn on feedback temperature control within the VI. Observe the measured temperature signal under feedback (closed-loop) control, which is displayed in the VI, for the next few minutes. If the measured temperature of the oil greatly overshoots the desired temperature, reacts too slowly to changes, or fails to converge to the desired set point, the user will need to adjust the control gains to achieve desired closed loop performance.

NOTE: The program defines a saturation limit for the power (and thus voltage) supplied to the resistive heating elements. For example, two elements reported herein consume up to 5 W power each. Wiring them in parallel means that total power consumption should not exceed 10 W. The user is advised to consider the maximum amount of power that should be supplied to the devices and know that this limit can affect the speed at which the closed-loop system will respond to desired temperature changes. Higher power heating elements enable faster heating and higher set point temperatures but require higher supplied currents for heating.

3.4. With the system tuned to acceptable closed-loop performance, enter the desired oil temperature for DIB formation as the set point in the VI.

NOTE: For example, a set point temperature of 60 °C yielded good results in experiments with BTLE liposomes in the aqueous droplets<sup>37</sup>. The user is referred elsewhere<sup>2,40</sup> for protocols explaining DIB assembly between droplets hanging on wire-type electrodes and configuration of electrophysiology equipment using the patch clamp amplifier, DAQ-1, and electrophysiology measurement software. Specifically, the protocol by Najem, et al.<sup>40</sup> can be closely followed until Step 13. Beyond that step, a slightly different approach is employed for successful monolayer and bilayer formation when using lipids that require heating to promote monolayer or bilayer formation.

3.5. Lower the tips of the silver/silver chloride (Ag/AgCl) electrodes into the oil until they nearly touch the bottom of the acrylic reservoir. This positioning of the electrode tips is crucial for keeping the droplet on the electrode in heated oil, where convective currents in the oil have been observed to detach droplets from the hydrogel-coated electrodes (**Figure 2c**).

3.6. Pipette a 250 nL droplet of aqueous lipid solution containing 2 mg/mL of BTLE, 100 mM



potassium chloride (KCl), and 10 mM 3-(N-morpholino) propanesulfonic acid (MOPS) onto each electrode tip and let them incubate in the heated oil for a minimum of 10 minutes to promote monolayer formation.

3.7. Cover the headstage and heated stage fixture with a grounded Faraday cage.

3.8. Bring the droplets into gentle contact by slowly manipulating the horizontal positions of the electrodes until the user sees the droplets deform from contact or begin to displace on another and wait a few minutes until bilayer formation commences. If after several minutes a bilayer has not formed, the droplets can be coerced together more to facilitate bilayer formation. The formation of a thinned interfacial bilayer can be confirmed through visual inspection (**Figure 5a**) or by measuring the increase in the amplitude of a square-waveform capacitive current induced by a waveform generator outputting a 10 mV, 10 Hz triangular voltage<sup>22</sup>. Allow the bilayer to equilibrate for a minimum of 10 minutes to reach a steady interfacial area, upon initial formation and prior to subsequent characterization at the initial set point.

NOTE: The type of oil can have a significant impact on bilayer thinning, membrane thickness, and inter-droplet contact angle. In general, the smaller the oil molecule the more easily it can remain in the hydrophobic core of the bilayer occupied by lipid acyl chains. Oil retention increases both monolayer and bilayer tensions and thickness and decreases the area and angle of contact between droplets. These metrics signify a weaker state of adhesion. Larger, bulkier molecules exert the opposite effect. For example, squalene is bulkier molecule than alkanes such as hexadecane, which enables it to be readily excluded from between monolayers during bilayer thinning. As such, DIBs formed in squalene are thinner, they display higher contact areas and angles, and they exhibit higher free energies of formation<sup>22,43</sup> (a measure of droplet-droplet adhesion).

#### 4. Characterization of temperature-dependent behaviors in DIBs

NOTE: Many physical processes can be studied in DIB-based model membranes, including how changes in temperature affect the structure and transport properties of the membrane. The following steps should be performed after successful bilayer formation at a desired temperature.

4.1. Measure the nominal capacitance of the membrane while lowering the temperature of the oil bath from a set point that permits bilayer formation to identify thermotropic phase transitions of the lipids in the membrane<sup>38</sup>.

4.1.1. Right click the **temperature graph** on the GUI and clear the displayed data. This ensures sufficient space in the buffer is available for subsequent recordings.

4.1.2. Using the waveform generator connected to the patch clamp amplifier, apply a triangular voltage waveform (e.g., 10 mV, 10 Hz) across the DIB electrodes and record the induced current response through the bilayer.

4.1.3. Cool the bilayer by reducing the set point temperature in 5 °C increments and waiting a minimum of 5 min at the new steady state temperature between temperature changes until the desired temperature is achieved. Alternatively, try passively cooling the bilayer by turning off feedback control system, however, experiments implementing passive cooling from 50-60 °C resulted higher rates of coalescence.

4.1.4. After the oil bath and bilayer cool to the desired minimum temperature, right click the temperature graph in the GUI again and export the temperature data versus time to a spreadsheet software. Stop the current recording.

4.1.5. From the measured current, calculate the nominal capacitance of the square wave-current response versus time during the cooling period.

4.1.6. Plot nominal capacitance ( $C$ ) versus temperature ( $T$ ) to observe how membrane capacitance changed. Locate nonmonotonic changes in  $C$  versus  $T$  to identify  $T_M$ .

NOTE: Nominal capacitance can be calculated from the amplitude of square-wave current<sup>44</sup>,  $|I|$  using the relationship,  $|I| = C dv/dt$ , where  $dv/dt$  is equal to four times the product of amplitude ( $A$ ) and frequency ( $f$ ) of the applied triangular voltage. From these equations,  $C = |I|/4Af$ .

4.2. Similarly, assess the quasi-static specific capacitance ( $C_m$ ) of the bilayer at fixed temperatures by successively incrementing the temperature of the oil bath and the bilayer area.

4.2.1. Change the set point temperature in 10 °C increments using the GUI and allow the system to equilibrate to the new temperature.

4.2.1.1. Perform Step 4.1.2 to initiate the measurement of capacitive current and recording.

4.2.1.2. Change the bilayer area by carefully adjusting the positions of the electrodes using the micro-manipulators (i.e., separating the electrodes reduces bilayer area). Allow for the square-wave current to reach a steady state amplitude and collect images of the DIB to enable calculation of membrane area versus time by using a camera mounted to the microscope to image the bilayer as seen from the aperture of the microscope stage. Simultaneously, add a digital tag in the current recording software to mark the corresponding timepoint for image collection.

NOTE: Micro-manipulators allow for the precise control of the electrodes and thus gentle contact between droplets. Coarse manipulation of the droplets can lead to a failed experiment by coalescence of the droplets or by causing a droplet to fall off the electrode. As discussed elsewhere<sup>22</sup>, bilayer area is calculated from the contact length between droplets, which appear as overlapping circles in a bottom-view image. The positions and dimensions of the droplets, and the length of the contact line, can be calculated using an image-processing software or with other

scientific programming tools.

4.2.1.3. Repeat Step 4.2.1.2 a minimum of 4 times to obtain a total of 5 DIB images and steady-state regions of bilayer current.

4.2.2. Repeat Step 4.2.1 at each desired temperature.

4.2.3. At the tagged timepoints corresponding to steady-state bilayer areas for acquired images, analyze the current recordings and DIB images to extract bilayer capacitance,  $C$ , and area,  $A$ , data for each temperature.

4.2.4. Plot  $C$  versus  $A$  data for each temperature and compute the slope of a first-order regression, which represents the specific capacitance,  $C_m$ , of the bilayer at each temperature<sup>22</sup>.

4.2.5. Plot values of  $C_m$  obtained from Step 4.2.4 versus their respective temperatures,  $T$ .

4.2.6. Examine the  $C_m$  versus  $T$  data for non-monotonic variations to identify melting temperatures,  $T_M$ .

4.3. Assess the dynamics of voltage-dependent ion channel formation by generating a dc voltage step input across the bilayer.

4.3.1. Set **Initial Voltage** to the desired step value in mV (e.g., 100 mV).

4.3.2. Set **Final Voltage** and **Step Size** to a value higher than the desired step (e.g., 110 mV final voltage and 10 mV step size).

4.3.3. Set a desired duration time for the step input in seconds (e.g., 90 s).

4.3.4. Choose the desired polarity for the step input (e.g., positive).

4.3.5. Switch the patch clamp amplifier to send to the headstage the command voltage originating from LabView/voltage output module.

4.3.6. Initiate current recordings.

4.3.7. Turn on the voltage and record the induced current response, which should exhibit an S-shaped response to a critical voltage (e.g., ~70 mV for 1  $\mu$ g/mL Mz in 2 mg/mL BTLE).

4.4. Separately, dynamic current-voltage relationships for a membrane can be obtained at desired temperatures to reveal voltage-dependent relationships, such as ion channel behaviors.

4.4.1. Switch the patch clamp amplifier to send to the headstage the command voltage originating from the waveform generator and initiate current recordings.

442 4.4.2. On the waveform generator, output a continuous sinusoidal waveform with a desired  
443 amplitude, offset, and frequency.

445 4.4.3. Record the induced current response across one or multiple cycles.

447 4.4.4. Repeat as desired for different sine wave amplitudes and frequencies and  
448 temperatures.

450 (Place Figure 3 here)

#### 452 REPRESENTATIVE RESULTS:

454 **Figure 1** shows how the aluminum fixture and acrylic oil reservoir are prepared on the  
455 microscope stage for DIB formation. Assembly steps 1.2-1.4 serve to thermally insulate the  
456 fixture from the stage for more efficient heating. Steps 1.5-1.7 show how to properly attach the  
457 thermocouple to the fixture and position the oil reservoir, and steps 1.8 -1.9 show recommended  
458 locations for dispensing oil into these pieces.

460 **Figure 2** outlines the components used to establish feedback temperature control and perform  
461 electrical measurements on a DIB: a PC, an HP fixed gain power amplifier, a patch clamp amplifier  
462 and a DAQ system (or equivalent instrument for applying voltage and measuring pA-nA level  
463 currents), a second DAQ with appropriate analog inputs and outputs, a waveform generator, and  
464 the assembled aluminum fixture with attached resistive heaters. DAQ-2 makes use of two  
465 modules (**Figure 2b**). A 4-channel,  $\pm 10$  V, 16-bit analog voltage output module used to initiate  
466 the independent voltages supplied to the input of the power amplifier (blue connection in **Figure**  
467 **2a**) and an Eternal Command input on the patch clamp amplifier (green connection). The voltage  
468 output module is limited by a maximum output current of 46 mA and a maximum output voltage  
469 of 10 V, whereas each heating element used herein consumes as much as 5 W of power (~180  
470 mA max) at a maximum voltage of 28 V. For this reason, the power supply/amplifier was included  
471 to pre-amplify the output voltage and supplement the supplied current needed for powering the  
472 heating elements (wired in parallel) attached to the aluminum fixture. A 4-channel, 24-bit  
473 thermocouple input device used to digitize temperature measurements from the oil reservoir  
474 near the DIB (yellow connection). Since the thermocouple input device module allows up to 4  
475 thermocouples, the user may consider monitoring temperatures at other locations in the fixture.  
476 If done, they will also need to consider which signal or combination of signals is used for  
477 comparison to the desired set point temperature within the feedback loop.

479 These outputs and measured signals are controlled via two software: 1) the custom GUI for  
480 temperature control; and 2) electrophysiology measurement software for DIB electrophysiology.  
481 **Figure 3** shows a screenshot of the GUI and includes annotations to corresponding steps in the  
482 protocol. The GUI is used to define key parameters (Set Point temperature, PI control gains,  
483 voltage limits), compare the measured temperature to the set point temperature and compute  
484 the control signal supplied to the amplifier and then the heating elements, and record data of

the temperature and applied voltage versus time. This program also includes the ability to command the voltage applied to DIB electrodes (**Figure 2c**) via the patch clamp amplifier. Separately, measurement software is used to configure measurements of both the voltage applied to the DIB electrodes and the induced current through the lipid bilayer. A voltage proportional to DIB current is output by the patch clamp amplifier and sent via BNC cable to DAQ-1 (connection not shown).

**Figure 4** plots the change in temperature and absolute electrical power sent to the heaters versus time under both open-loop and closed-loop heating scenarios. For the former, an arbitrary input voltage corresponding to  $\sim 5.2$  W of power was applied to the heaters, which resulted in an exponential rise in temperature with a time constant of  $\sim 125$  s and a steady state  $\Delta T \approx 4.5$  °C/W after an initial delay of  $\sim 20$  s. These characteristics of the open-loop system were used to construct a model of the closed-loop system in a simulation software (see **Figure S4** for details) that can be used to determine values for the proportional and integral control gains. The closed-loop and simulated model responses in **Figure 4** thus represent the measured and simulated responses of the tuned PI controller, with  $K_p$  and  $K_i$  values of 0.598 and 0.00445, respectively, to a set point temperature 20 °C higher than RT. Compared to the open-loop case, both the simulation and the measurements confirm the increased speed of response in the closed-loop system (time constant  $\sim 63$  s). The reduction in heating time comes at the expense of higher initial applied power and desired set point and the measured oil temperature remained within 0.6 °C at steady state, which was deemed suitable for use. Total supplied power is limited within the program during closed-loop control so as not to eclipse the 10 W total power limit for the two heaters.

The temperature control system was used to showcase the temperature-dependence of solvent in a DIB formed from BTLE lipids and its impact on membrane capacitance (**Figure 5**). BTLE lipids were chosen for this measurement because heating is required for DIB formation due to a lipid phase transition that occurs between 35-42 °C<sup>38</sup>. The protocol described herein was performed to initiate bilayer formation at 60 °C. Following membrane formation and equilibration, the temperature can be successively lowered or raised as needed to characterize the response of the membrane. For example, **Figure 5a** shows representative measurements of raw capacitive current (square-shaped waveform) and temperature versus time during a heating cycle from RT to  $\sim 60$  °C. Observe that the amplitude of the capacitive current waveform reduces by more than half as temperature rises, which is caused by the uptake of oil into the hydrophobic core of the membrane. This change thickens the interface and alters the lateral tension of the bilayer<sup>22,37,38,45</sup>.

The data in **Figure 5b** document changes in nominal capacitance,  $C$ , (normalized by the capacitance at 27 °C) versus temperature,  $T$ , across one complete cooling-heating cycle after initial bilayer formation at 60 °C. Just like in **Figure 5a**, as temperature rises, capacitance drops. However, what this presentation shows more clearly are the nonmonotonic changes that occur at temperatures between  $\sim 30$ -42 °C, which represents the collective melting temperature,  $T_M$ , during which the lipid mixture transitions between a liquid-ordered and a liquid-disordered thermotropic phase. The temperature where the nonmonotonic change in capacitance occurs

corresponds to a change in bilayer thickness from exclusion of oil from the membrane<sup>38</sup>. Also, note that the hysteresis shown between the heating cycle and the cooling cycle is due to irreversible changes in bilayer area that occur between subsequent cycles, which were typically performed 10 min apart.

Similarly, **Figures 6a,b** show how quasi-static measurements of specific capacitance,  $C_m$ , at different temperatures can be used to identify  $T_M$ . Here, the area of the membrane is varied successively by manually increasing the distance between the droplet electrodes. During this experiment, the droplets are first pushed together to promote maximum membrane area prior to subsequent reductions in contact area with stepwise separations between the electrodes. At each level of contact, the nominal capacitance of the bilayer ( $C$ ) is assessed from the induced current and its area ( $A$ ) is determined through image analysis. Plotting  $C$  versus  $A$  allows for a linear regression, where the slope represents the value of  $C_m$  as shown in **Figure 6a**. Repeating this procedure across multiple temperatures (**Figure 6b**) shows that  $C_m$  decreases by nearly 50% at temperatures above  $T_M$ , confirming an increase in the hydrophobic thickness of the membrane due to heating-induced hexadecane uptake (see **Figure S5** for complete  $C$  versus  $A$  data). At higher temperatures, the additional solvent in the membrane also reduces the maximum contact area between the droplets, and thus maximum nominal capacitance. Reducing the temperature reverses these effects. The DIB image in **Figure 6c** shows that when the temperature (25 °C) is well below  $T_M$ , the membrane can stably adopt a highly adhesive state—even under the tension of stretched droplets caused by well-separated electrodes. This is the result of complete exclusion of hexadecane from the bilayer, which increases the adhesion energy of the droplets. In this state, the bilayer area cannot be reliably changed through manipulation of the electrodes and hinders the ability to accurately measure specific capacitance (see **Figure S5** for more details).

Finally, the representative data in **Figure 7** show how temperature changes can affect the behaviors of pore-forming species that create ion conducting channels through a DIB. Monazomycin (Mz), a positively-charged antibiotic that forms cation selective channels through the bilayer at sufficient transmembrane potentials<sup>37,46</sup>, was chosen to demonstrate this relationship. These measurements were conducted on a BTLE-based (2 mg/mL final concentration in both droplets) DIB doped with Mz (1 µg/mL final concentration in both droplets). The current versus voltage traces shown in **Figure 7a** were obtained by applying sinusoidal membrane voltages and measuring the induced current at two different temperatures; the arrows and subsequent numbers in **Figure 7a** aid in visualizing the successive quarters of the sinusoidal voltage with respect to time. This type of measurement is often performed to examine the voltage-dependence of current through ion channels. The data here show that increasing the temperature of the DIB from 27 °C to 45 °C causes the threshold for channel formation to rise from  $\sim|100\text{ mV}|$  to  $\sim|110\text{ mV}|$ . This change, likely driven by the higher membrane thickness due to absorbed oil, shows that the energy barrier for insertion has risen. The hysteresis in these curves—which signifies memory resistance—can be caused by voltage-induced changes in either bilayer area or the kinetics of Mz channel formation and inactivation<sup>47</sup>.

To help separate these factors in DIBs, transient changes in ion current can be measured in

response to a DC step voltage. **Figure 7b** shows the measured current density for the same Mz-doped BTLE membrane at the same voltage level (+90 mV) and two different temperatures (27 °C and 45 °C). The data show clearly that the kinetics of the channel responses are quite different. Notably, at 27 °, the membrane exhibits a faster, larger increase in current that is then followed by a transient decay (the latter is a result of Mz channels translocating across the bilayer to an inactive state<sup>47</sup>). The response is much more muted at 45 °C, where the S-shaped rise in current is not preceded by a subsequent drop. Differences such as these are helpful for assessing the kinetics of channel responses and understanding how these could contribute to the total dynamic resistance of the membrane.

## FIGURES AND TABLES:

**Figure 1: Heated stage assembly.** Images show the assembly of the thermally conductive fixture and oil reservoir for DIB formation; numbers beneath each image identify the corresponding step of the protocol.

**Figure 2: System wiring connections.** A schematic of the devices and wiring required for the system is shown in (a), while a detailed look at the DAQ-2 connections is provided in (b). The illustration in (c) shows aqueous droplets on hydrogel-coated electrodes submerged in oil for DIB formation (c). The two electrodes are connected to the grounded and ungrounded (V+) connections, respectively, on the headstage unit of the patch clamp amplifier.

**Figure 3: The temperature control VI.** This figure highlights and labels the critical steps required to use the program's GUI to control the temperature of the oil bath.

**Figure 4: Open-loop versus closed-loop heating.** Panel (a) compares the time responses for the measured and simulated (See SI) closed-loop system to a +20 °C temperature step to the open-loop heating response under fixed applied power. Panel (b) displays the power dissipated by each system.

**Figure 5: Measuring capacitance and varying temperature.** The typical square waveform current response to a 10 mV, 10 Hz triangular waveform input on a BTLE lipid membrane undergoing a phase transition is shown in (a). The phase transition of the lipids can also be seen in the area measurement data displayed above panel (a). Capacitance normalized by initial capacitance at 27 °C is shown in panel (b) plotted as a function of temperature for a heating and cooling cycle.

**Figure 6: Specific capacitance measurements** Panel (a) shows nominal capacitance versus bilayer area obtained at successive contact areas for two different temperatures. Linear regressions to each set are used to determine their respective values of  $C_M$ . Panel (b) plots  $C_M$  versus  $T$ , while panel (c) shows the stable capacitive current waveform (left) and contact area (right) under attempted droplet separation at 25 °C.

**Figure 7: Voltage-dependent membrane resistance and Mz ion-channel kinetics versus**

**temperature.** Panel (a) shows how the current-voltage relationship changes with temperature for BTLE DIBs formed between droplets containing 1  $\mu\text{g}/\text{ml}$  Mz. The arrows and numbers represent the successive portions of the applied sine wave. The differences in these traces illustrate how temperature shifts the voltage threshold for Mz insertion, which is identified as the magnitude of the voltage where induced current increases sharply. Likewise, panel (b) shows the impact temperature has on the transient current response induced by a DC step voltage of 90 mV.

**Figure S1: Aluminum fixture.** This drawing shows the necessary dimensions and features for fabrication of the aluminum fixture that is the base of the heated stage. The 25.2 mm X 26 mm flat spots adjacent to the oil well were designed to allow for a maximal amount of surface-area contact between the fixture and the heating elements for heat conduction. Likewise, aluminum was chosen for the base fixture material due to its high thermal conductivity. The M3 X 0.5 mm screw hole called out in the print is used to secure and position the thermocouple in the oil well.

**Figure S2: Acrylic substrate.** The acrylic substrate is relatively simple piece to fabricate, with no critical outstanding features, except for the profile. The exterior profile was designed with Poka-yoke in mind so the acrylic substrate can only be oriented in the fixture in such a way to allow ample room for the thermocouple to fit in the oil well.

**Figure S3: Heated stage assembly.** An exploded view of the assembled heated stage has been provided to aid the experimenter during initial setup. Also, take note of the area highlighted by the dashed circle, as this is the ideal position to fill the aluminum fixture with oil during protocol step 1.8.

**Figure S4: Open loop data and Simulink modeling panel.** (a) shows the open-loop temperature responses to varying dc power levels that were used to assess the delay time,  $t_d$ , the time constant,  $\tau$ , and open-loop heating gain,  $\alpha$ , of the system. The delay time represents the time lag Thermal Insulation Layer (Top) Acrylic Reservoir Heating Element Thermal Insulation Layer (Bottom) M3 Screw Glass Coverslip Fill Location before temperature starts rising ( $\sim 20$  s). Each value of  $\tau$  (marked by \*,  $\sim 125$  s) is defined as the time required for 63.2% of the total rise in temperature to occur. Panel (b) shows the steady state change in temperature ( $\Delta T$ ) versus the applied power. The slope of the data plotted in (b) was used to compute the  $\alpha$ , which represents the ratio of temperature change per supplied power. These parameters were used in the Simulink model shown in panel (c) and provided as a supplementary file to tune the PI controller to achieve a desired closed-loop temperature control response.

**Figure S5: Additional specific capacitance data.** The plots shown in **Figure 6a,b** were compiled from this specific-capacitance ( $CM$ ) data set. This plot also showcases the inability to accurately measure capacitance at temperatures of 25  $^{\circ}\text{C}$  and below, therefore this measurement was excluded from the dataset. The area changes necessary for an accurate  $CM$  measurement require excessive force to be applied to the droplets from the micromanipulators, which causes severe distortion of the droplets shape and area of contact.



## DISCUSSION:

The protocol described herein provides instructions for assembling and operating an experimental system to control the temperature of the oil and droplets used to form DIBs. It is especially beneficial for enabling DIB formation using lipids that have melting temperatures above RT. Moreover, by precisely varying the temperature of the oil reservoir, the bilayer temperature can be manipulated to study the effects of elevated temperatures on various membrane properties and characteristics, including capacitance, area, thickness, induced thermotropic-phase changes, kinetics of membrane-active species, and the energetics of adhesion of the bilayer interface<sup>37,38</sup>.

The protocol consists of three parts prior to use in a DIB study: 1) preparation and assembly of the heated stage fixture; 2) connecting the various instruments; and 3) confirming suitable temperature control performance with the chosen proportional and integral control gains. Most important in part 2, the user must make sure to avoid shared conduction paths between the output of power amplifier (>mA currents) and the patch clamp headstage (pA-nA currents). An inadvertent short could cause permanent damage to the headstage. Additionally, ensuring that the PC and all instruments are connected to a common AC power ground, and the use of a grounded Faraday cage near the headstage and droplet electrodes helps to minimize noise in bilayer current measurements. After setup in part 2 is complete, the user must first assess the open-loop heating response of the oil reservoir by applying a fixed voltage to the heating elements and recording the subsequent rise in temperature (like shown in **Figure 4a**). This type of exponential response can be used to define and simulate a simple model of the closed-loop system for varying values of control gains (see **Figure S4** for details). The control gains reported herein allow the system to heat to a desired temperature level quickly (~ 2 minutes) and with little overshoot and maintain set point value accurately. But the specific gains required will depend on the power level of the heating elements as well as the geometry of the fixture that supports the oil reservoir. Once suitable values of control gains are determined and the feedback control system operates as desired, the user may then begin to assemble and characterize a DIB.

The protocol does not change the process of DIB formation or characterization, however there are limitations and considerations. Raising the temperature of the oil can affect how droplets hang on the electrodes, due to reductions in monolayer tension and oil density that increase droplet sagging and convective currents in the oil that can move the droplets. Hence, the protocol suggests lowering the tips of the electrodes to near the bottom surface of the substrate such that droplets are supported and held still by the acrylic reservoir. The user should assess how much the substrate may be distorting the droplets (if lowered too far), and consider this distortion when calculating of the area of the bilayer from images of DIBs as discussed elsewhere<sup>22</sup>.

While the described system is limited to heating of the oil bath, a Peltier cooling device could be used in place of the resistive heating elements if testing at temperatures below RT is needed. In this case, however, the user will need to consider the freezing point of the oil phase. Many alkanes freeze at temperatures higher than 0 °C; hexadecane described herein freezes at 18 °C. If the oil freezes, droplets will no longer be moveable and a bilayer between droplets may become

unstable or rupture.

For a previously untested lipid composition, key unknowns are the incubation time and temperature required to enable sufficient monolayer assembly at the surfaces of the droplets. The general rule is to heat the oil to a temperature above  $T_M$ , where lipid mobility is enhanced allowing for faster lateral diffusion and tighter packing at the oil-water interface<sup>48</sup>, and wait long enough such that monolayer packing at the oil-water interface is high. The user may review published literature or consider their own complementary measurements to determine suitable time and temperature values: interfacial tension measurements on a pendant drop goniometer can be used to assess the time required for monolayer assembly<sup>49</sup> and differential scanning calorimetry is often used to identify thermotropic transitions of lipids<sup>38</sup>. Or an iterative approach may be pursued to identify suitable time and temperature where bilayer formation is consistent, the membrane is stable for more than a few minutes, and the resistance of the bilayer is  $>1\text{ G}\Omega$ . In recent studies with *E. coli* total lipid extract (ETLE)<sup>37</sup> and BTLE<sup>38,50</sup> a starting temperature  $>50\text{ }^\circ\text{C}$  consistently leads to stable bilayer formation. Similarly, the minimum stable temperature after DIB for a given lipid type may also vary between lipid selections. For example ETLE DIBs can be cooled to  $25\text{ }^\circ\text{C}$ <sup>37,45</sup>, whereas single component DPPC DIBs always coalesced below  $T_M \sim 40\text{ }^\circ\text{C}$ <sup>38</sup>. Observation has shown that BTLE DIBs show that  $27\text{ }^\circ\text{C}$  is a safe minimum temperature for maintaining a stable bilayer.

Our representative results show that changes in temperature can greatly affect the properties of the resulting DIB. The data in **Figure 5** shows that the nominal capacitance of the membrane decreases as temperature rises. Because capacitance,  $C$ , is directly proportional to bilayer area,  $A$ , and inversely proportional to thickness,  $d$ , as given by

$$C = \frac{\epsilon A}{d}, \quad (1)$$

a decrease in  $C$  can be manifest by a decrease in  $A$ , an increase in  $d$ , or both (assuming a fixed dielectric permittivity,  $\epsilon$ ). These relationships motivate the use of capacitance measurements and DIB images to assess changes in  $C$ ,  $A$ , and  $C_m$  versus temperature to determine which effects are significant. The data included in **Figure 5** and **Figure 6** for BTLE DIBs shows that both  $C$  and  $C_m$  (which represents the ratio  $\epsilon/d$ ) decrease by nearly 50% as temperature rises from  $30\text{ }^\circ\text{C}$  to  $60\text{ }^\circ\text{C}$ . Together, these indicate that higher temperature thickens the bilayer, due to an increased solubility of the acyl chains of the lipids in hexadecane<sup>51</sup>. The additional oil in the membrane can also affect the interfacial tension of the bilayer and the contact angle between droplets<sup>22,38</sup>. These effects can be quantified by analyzing images of a DIB at user-specified time intervals to monitor bilayer area and contact angle during heating and cooling.

The temperature favorability of oil in the membrane can also be used to assess thermotropic melting temperatures of the lipids and affect ion channel kinetics. The melting temperature for a lipid mixture can be defined by locating nonmonotonic changes in  $C$  versus  $T$  relationships as in **Figure 6**. The current measurements in **Figure 7** further reveal that temperature-induced changes in phase (i.e. fluidity) and thickness can impact the threshold voltage for insertion of ionophores like Mz. These physical associations are important for understanding ion channel behaviors in

model membranes, especially in scenarios aimed at replicating body temperature environments. However, they may also be useful for tuning the conductivity of the bilayer in applications such as neuromorphic computing devices<sup>50</sup>. For example, increased channel kinetics are a desirable feature when fabricating devices exhibiting memory resistance that need to mimic the speed, functionality, and short-term plasticity of the brain.

#### ACKNOWLEDGMENTS:

Financial support was provided by the National Science Foundation Grant CBET-1752197 and the Air Force Office of Scientific Research Grant FA9550-19-1-0213.

#### DISCLOSURES:

The authors have no conflicts of interests.

#### REFERENCES:

1. van Meer, G., de Kroon, A. I. P. M. Lipid map of the mammalian cell. *Journal of Cell Science*. **124** (1), 5-8 (2011).
2. Bayley, H. et al. Droplet interface bilayers. *Molecular BioSystems*. **4** (12), 1191-1208 (2008).
3. Hwang, W. L., Chen, M., Cronin, B., Holden, M. A. Bayley, H. Asymmetric droplet interface bilayers. *Journal of the American Chemical Society*. **130** (18), 5878-5879 (2008).
4. Holden, M. A., Needham, D., Bayley, H. Functional bionetworks from nanoliter water droplets. *Journal of the American Chemical Society*. **129** (27), 8650-8655 (2007).
5. Sarles, S. A., Leo, D. J. Physical encapsulation of droplet interface bilayers for durable, portable biomolecular networks. *Lab on a Chip*. **10** (6), 710-717 (2010).
6. Stanley, C. E. et al. A microfluidic approach for high-throughput droplet interface bilayer (DIB) formation. *Chemical Communications*. **46** (10), 1620-1622 (2010).
7. Gross, L. C. M., Heron, A. J., Baca, S. C., Wallace, M. I. Determining membrane capacitance by dynamic control of droplet interface bilayer area. *Langmuir*. **27** (23), 14335-14342 (2011).
8. Huang, J., Lein, M., Gunderson, C., Holden, M. A. Direct quantitation of peptide-mediated protein transport across a droplet,äinterface bilayer. *Journal of the American Chemical Society*. **133** (40), 15818-15821 (2011).
9. Leptihn, S., Thompson, J. R., Ellory, J. C., Tucker, S. J., Wallace, M. I. In vitro reconstitution of eukaryotic ion channels using droplet interface bilayers. *Journal of the American Chemical Society*. **133** (24), 9370-9375 (2011).
10. Castell, O. K., Berridge, J., Wallace, M. I. Quantification of membrane protein inhibition by optical ion flux in a droplet interface bilayer array. *Angewandte Chemie International Edition*. **51** (13), 3134-3138 (2012).
11. Dixit, S. S., Pincus, A., Guo, B., Faris, G. W. Droplet shape analysis and permeability studies in droplet lipid bilayers. *Langmuir*. **28** (19), 7442-7451 (2012).
12. Elani, Y., deMello, A. J., Niu, X., Ces, O. Novel technologies for the formation of 2-D and 3-D droplet interface bilayer networks. *Lab on a Chip*. **12** (18), 3514-3520 (2012).
13. Michalak, Z., Fartash, D., Haque, N., Lee, S. Tunable crystallization via osmosis-driven transport across a droplet interface bilayer. *CrystEngComm*. **14** (23), 7865-7868, (2012).

791 14. Punnamaraju, S., You, H., Steckl, A. J. Triggered release of molecules across droplet  
792 interface bilayer lipid membranes using photopolymerizable lipids. *Langmuir*. **28** (20), 7657-7664  
793 (2012).

794 15. Boreyko, J. B., Mruetusatorn, P., Sarles, S. A., Retterer, S. T., Collier, C. P. Evaporation-  
795 induced buckling and fission of microscale droplet interface bilayers. *Journal of the American*  
796 *Chemical Society*. **135** (15), 5545-5548 (2013).

797 16. Leptihn, S. et al. Constructing droplet interface bilayers from the contact of aqueous  
798 droplets in oil. *Nature Protocols*. **8** (6), 1048-1057 (2013).

799 17. Villar, G., Graham, A. D., Bayley, H. A Tissue-like printed material. *Science*. **340** (6128), 48-  
800 52 (2013).

801 18. Barriga, H. M. G. et al. Droplet interface bilayer reconstitution and activity measurement  
802 of the mechanosensitive channel of large conductance from *Escherichia coli*. *Journal of The Royal*  
803 *Society Interface*. **11** (98), (2014).

804 19. Boreyko, J. B., Polizos, G., Datskos, P. G., Sarles, S. A., Collier, C. P. Air-stable droplet  
805 interface bilayers on oil-infused surfaces. *Proceedings of the National Academy of Sciences*. **111**  
806 (21), 7588-7593 (2014).

807 20. Mruetusatorn, P. et al. Dynamic morphologies of microscale droplet interface bilayers.  
808 *Soft Matter*. **10** (15), 2530-2538 (2014).

809 21. Najem, J., Dunlap, M., Sukharev, S., Leo, D. J. The gating mechanism of mechanosensitive  
810 channels in droplet interface bilayers. *MRS Proceedings*. 1755, Cambridge University Press  
811 (2015).

812 22. Taylor, G. J., Venkatesan, G. A., Collier, C. P., Sarles, S. A. Direct in situ measurement of  
813 specific capacitance, monolayer tension, and bilayer tension in a droplet interface bilayer. *Soft*  
814 *Matter*. **11** (38), 7592-7605 (2015).

815 23. Bayley, H., Cazimoglu, I. Hoskin, C. E. G. Synthetic tissues. *Emerging Topics in Life Sciences*.  
816 **3** (5), 615-622 (2019).

817 24. Oliver, A. E. et al. Protecting, patterning, and scaffolding supported lipid membranes using  
818 carbohydrate glasses. *Lab on a Chip*. **8** (6), 892-897 (2008).

819 25. Maglia, G. et al. Droplet networks with incorporated protein diodes show collective  
820 properties. *Nature Nanotechnology*. **4** (7), 437-440 (2009).

821 26. Najem, J. S. et al. Activation of bacterial channel MscL in mechanically stimulated droplet  
822 interface bilayers. *Scientific Reports*. **5**, 13726 (2015).

823 27. Freeman, E. C., Najem, J. S., Sukharev, S., Philen, M. K., Leo, D. J. The mechanoelectrical  
824 response of droplet interface bilayer membranes. *Soft Matter*. **12** (12), 3021-3031 (2016).

825 28. Tamaddon, N., Sarles, S. A. Toward cell-inspired materials that feel: measurements and  
826 modeling of mechanotransduction in droplet-based, multi-membrane arrays. *Bioinspiration &*  
827 *Biomimetics*. **11** (3), 036008 (2016).

828 29. Restrepo Schild, V. et al. Light-patterned current generation in a droplet bilayer array.  
829 *Scientific Reports*. **7**, 46585 (2017).

830 30. Miliana, P. J., Muzzio, M., Denver, J., Cawley, G., Lee, S. Water permeability across  
831 symmetric and asymmetric droplet interface bilayers: Interaction of cholesterol sulfate with  
832 DPhPC. *Langmuir*. **31** (44), 12187-12196 (2015).

833 31. Mruetusatorn, P. et al. Control of membrane permeability in air-stable droplet interface  
834 bilayers. *Langmuir*. **31** (14), 4224-4231 (2015).

- 835 32. Wauer, T. et al. Construction and manipulation of functional three-dimensional droplet  
836 networks. *ACS Nano*. **8** (1), 771-779 (2013).
- 837 33. Bayley, H. Building blocks for cells and tissues: Beyond a game. *Emerging Topics in Life*  
838 *Sciences*. **3** (5), 433-434 (2019).
- 839 34. Booth, M., Restrepo Schild, V., Downs, F. Bayley, J. Droplet network, from lipid bilayer to  
840 synthetic tissues. in *Encyclopedia of Biophysics*. Springer. (2019).
- 841 35. Booth, M. J., Cazimoglu, I., Bayley, H. Controlled deprotection and release of a small  
842 molecule from a compartmented synthetic tissue module. *Communications Chemistry*. **2** (1), 142,  
843 (2019).
- 844 36. Gobbo, P. et al. Programmed assembly of synthetic protocells into thermoresponsive  
845 prototissues. *Nature Materials*. **17** (12), 1145-1153 (2018).
- 846 37. Taylor, G. J., Sarles, S. A. Heating-enabled formation of droplet interface bilayers using  
847 *Escherichia coli* total lipid extract. *Langmuir*. **31** (1), 325-337 (2015).
- 848 38. Taylor, G. J. et al. Capacitive detection of low-enthalpy, higher-order phase transitions in  
849 synthetic and natural composition lipid membranes. *Langmuir*. **33** (38), 10016-10026 (2017).
- 850 39. Lee, S., Kim, D. H., Needham, D. Equilibrium and dynamic interfacial tension  
851 measurements at microscopic interfaces using a micropipet technique. 2. Dynamics of  
852 phospholipid monolayer formation and equilibrium tensions at the water-air interface. *Langmuir*.  
853 **17** (18), 5544-5550 (2001).
- 854 40. Au - Najem, J. S. et al. Assembly and characterization of biomolecular memristors  
855 consisting of ion channel-doped lipid membranes. *Journal of Visualized Experiments*. (145),  
856 e58998, (2019).
- 857 41. Najem, J. S. et al. Assembly and characterization of biomolecular memristors consisting  
858 of ion channel-doped lipid membranes. *Journal of Visualized Experiments*. (145), e58998 (2019).
- 859 42. Wang, Y.-G., Shao, H.-H. Optimal tuning for PI controller. *Automatica*. **36** (1), 147-152  
860 (2000).
- 861 43. Needham, D., Haydon, D. A. Tensions and free energies of formation of "solventless" lipid  
862 bilayers. Measurement of high contact angles. *Biophysical Journal*. **41** (3), 251-257 (1983).
- 863 44. Sarles, S. A., Leo, D. J. Physical Encapsulation of Interface Bilayers for durable portable  
864 biolayer network. *Lab on a Chip*. **10** (6), 710-717 (2010).
- 865 45. Taylor, G. J., Sarles, S. A. Heating-enabled formation of droplet interface bilayers using  
866 *Escherichia coli* total lipid extract. *Langmuir*. **31** (1), 325-337, (2014).
- 867 46. Muller, R. U., Peskin, C. S. The kinetics of monazomycin-induced voltage-dependent  
868 conductance. II. Theory and a demonstration of a form of memory. *The Journal of General*  
869 *Physiology*. **78** (2), 201-229 (1981).
- 870 47. Muller, R. U., Peskin, C. S. The kinetics of monazomycin-induced voltage-dependent  
871 conductance. II. Theory and a demonstration of a form of memory. *The Journal of General*  
872 *Physiology*. **78** (2), 201 (1981).
- 873 48. Nenner, A. et al. Independent mobility of proteins and lipids in the plasma membrane  
874 of *Escherichia coli*. *Molecular Microbiology*. **92** (5), 1142-1153 (2014).
- 875 49. Venkatesan, G. A. et al. Adsorption kinetics dictate monolayer self-assembly for both lipid-  
876 in and lipid-out approaches to droplet interface bilayer formation. *Langmuir*. **31** (47), 12883-  
877 12893 (2015).
- 878 50. Najem, J. S. et al. Memristive ion channel-doped biomembranes as synaptic mimics. *ACS*

879 *Nano.* **12** (5), 4702-4711 (2018).

880 51. Tamaddoni, N., Taylor, G., Hepburn, T., Michael Kilbey, S., Sarles, S. A. Reversible, voltage-  
881 activated formation of biomimetic membranes between triblock copolymer-coated aqueous  
882 droplets in good solvents. *Soft Matter.* **12**, 5096 - 5109 (2016).

883

Figure 1

[Click here to access/download;Figure;Figure 1.png](#)

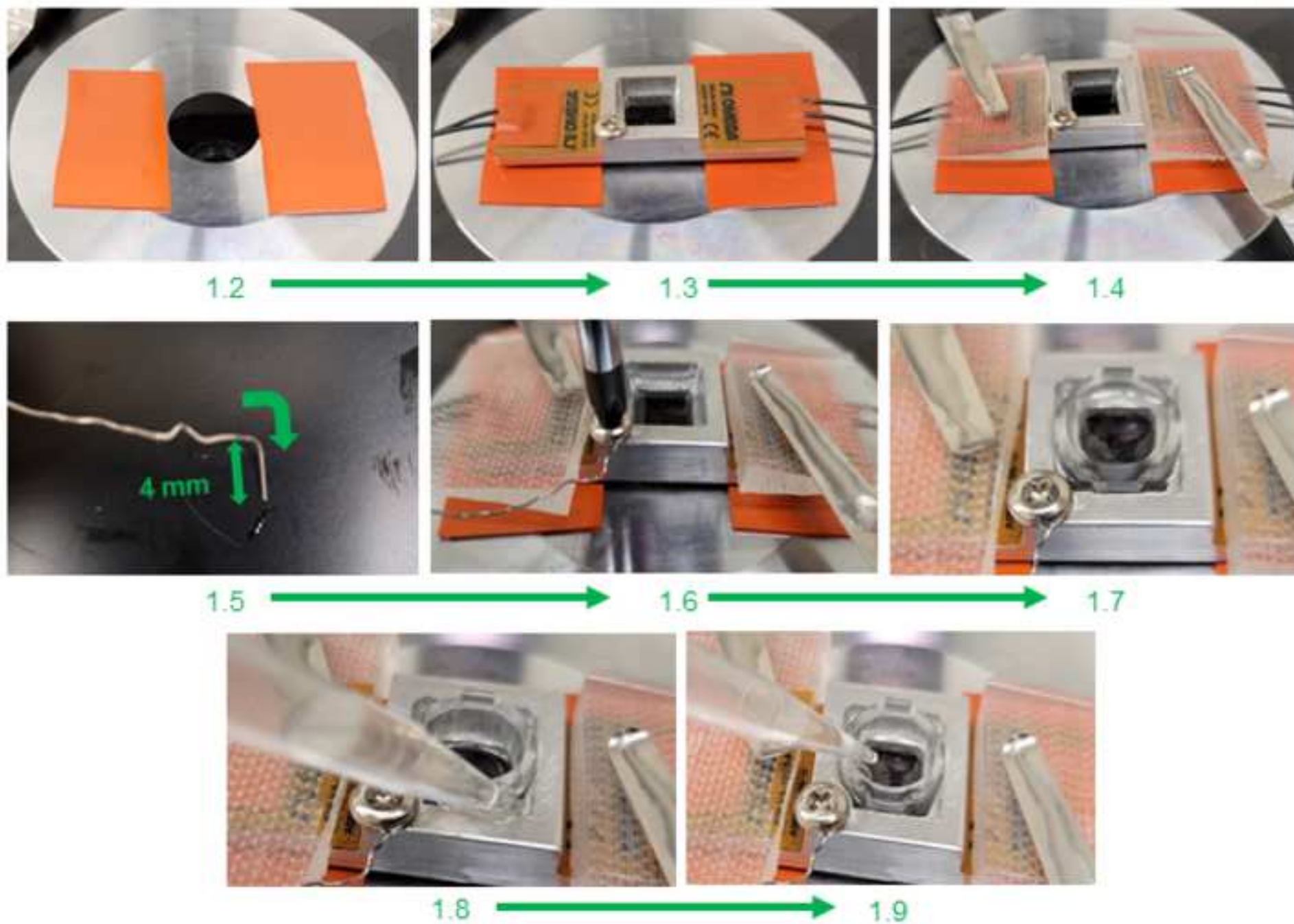




Figure 2

[Click here to access/download;Figure;Figure 2.png](#)

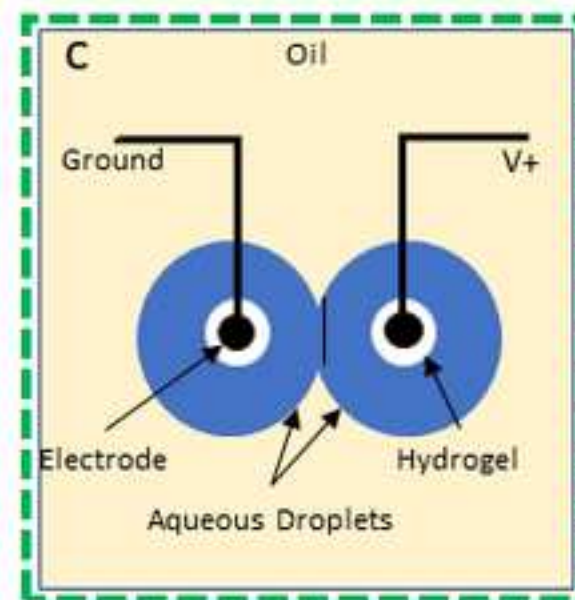
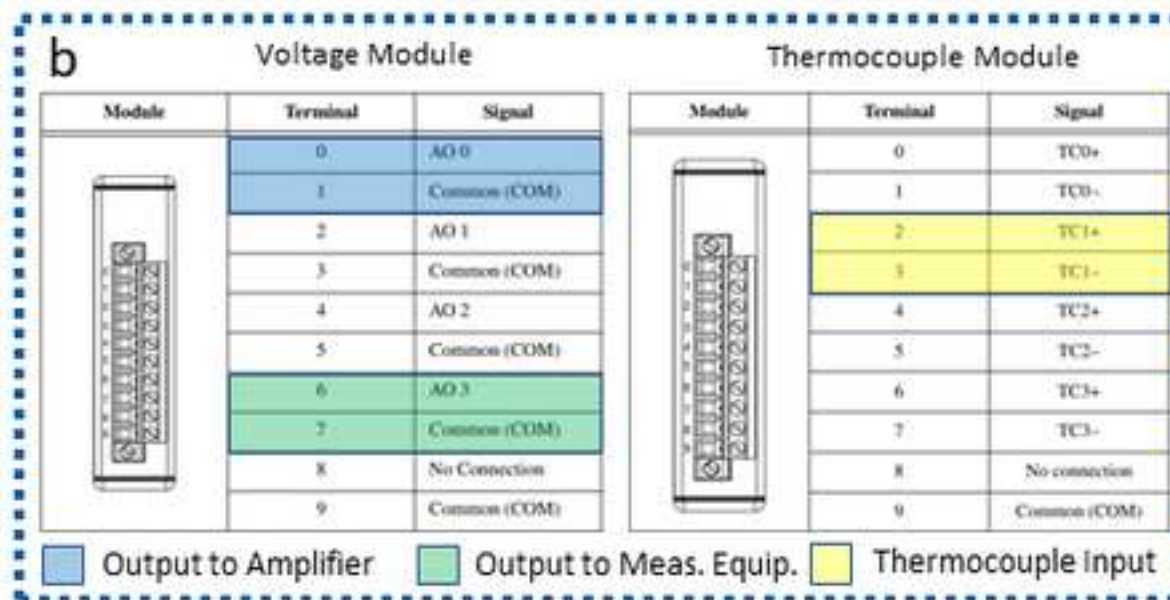
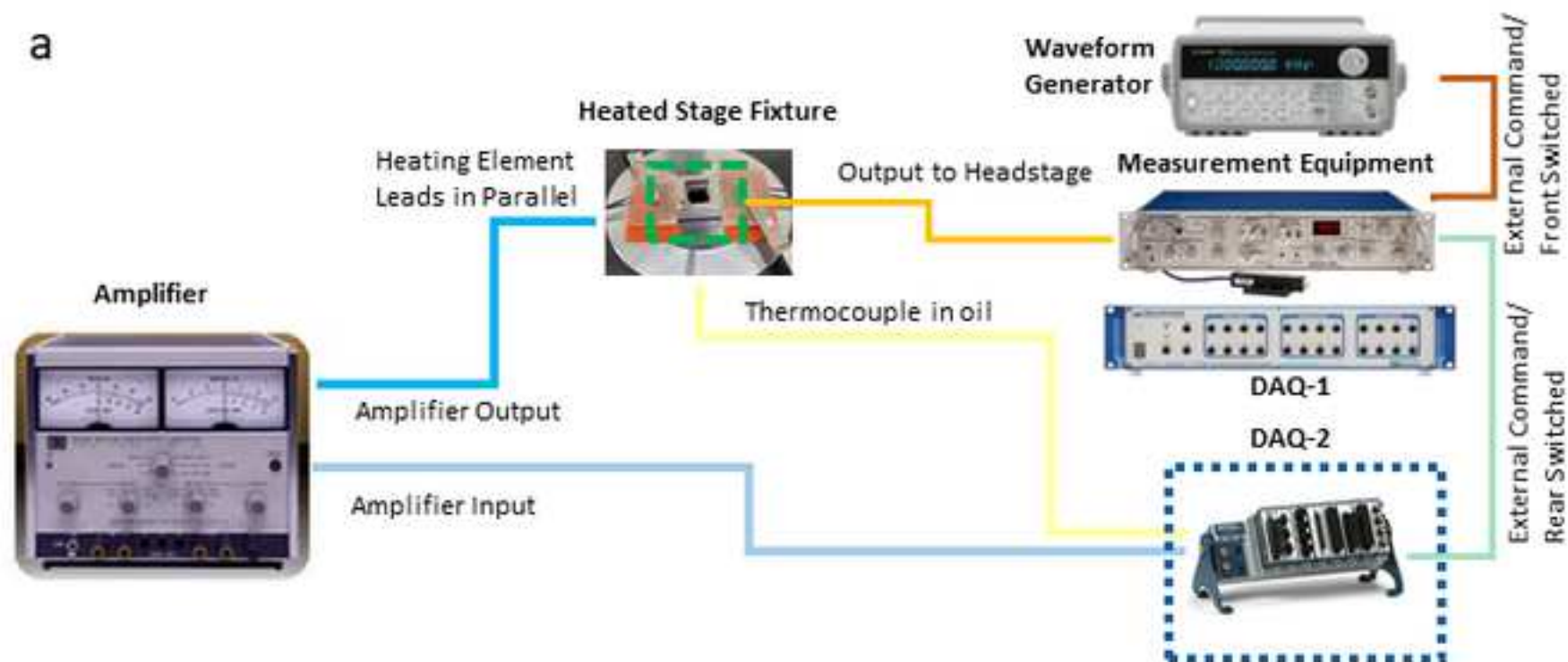




Figure 3

[Click here to access/download;Figure;Figure 3.png](#)

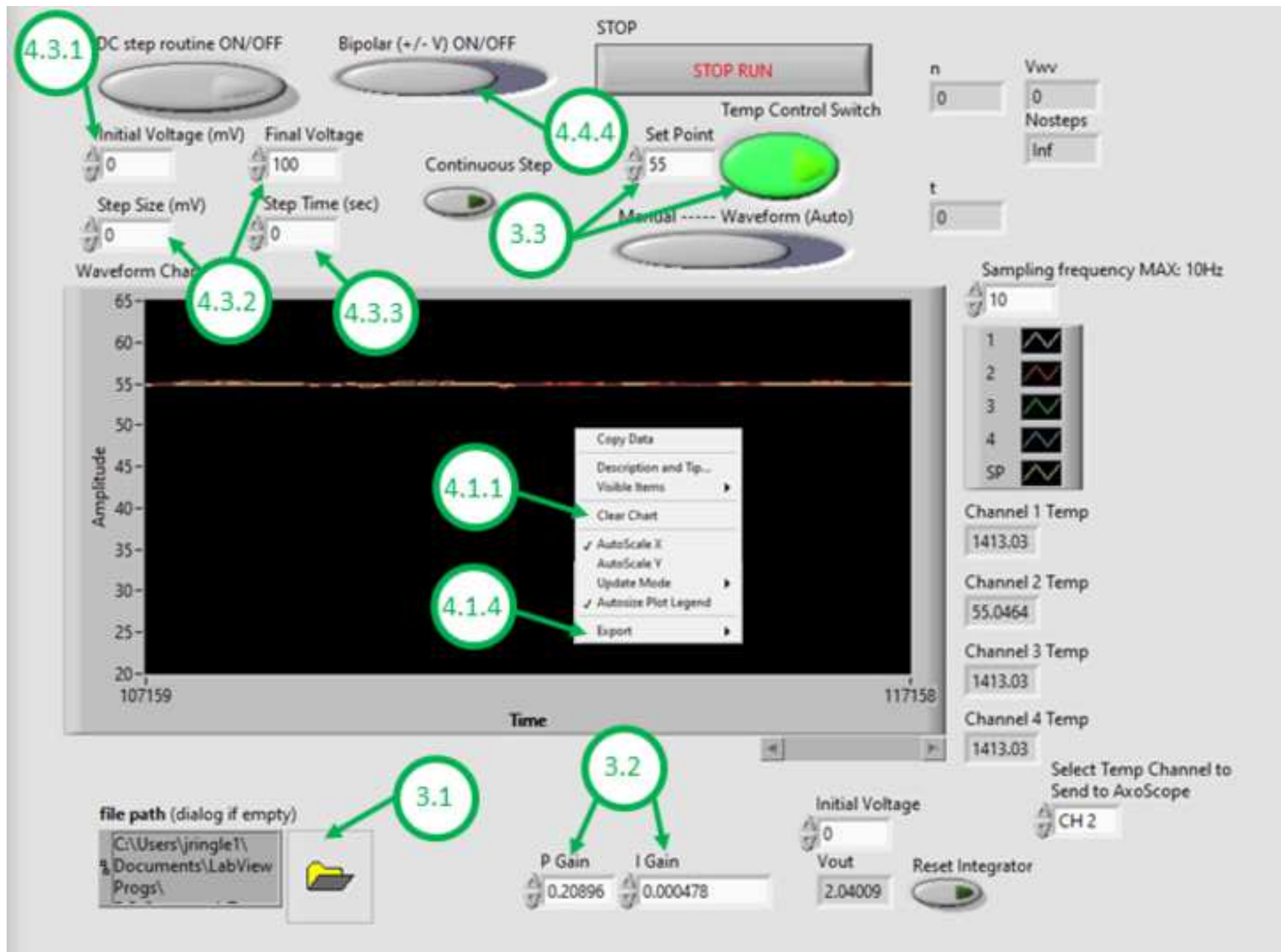


Figure 4

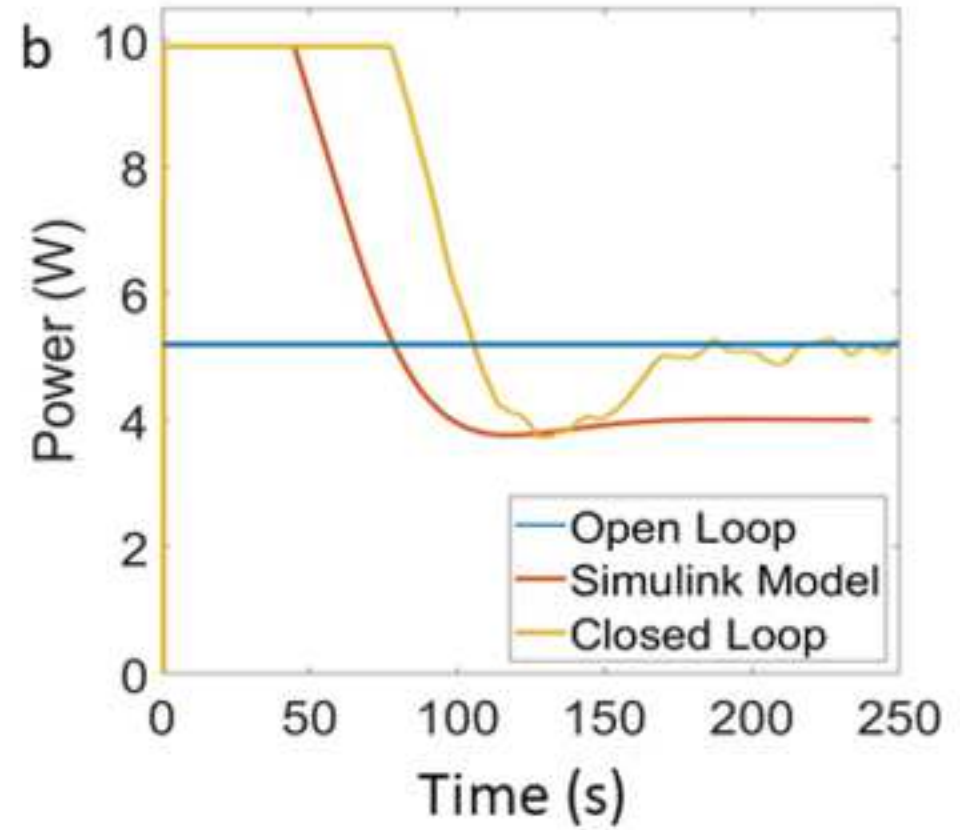
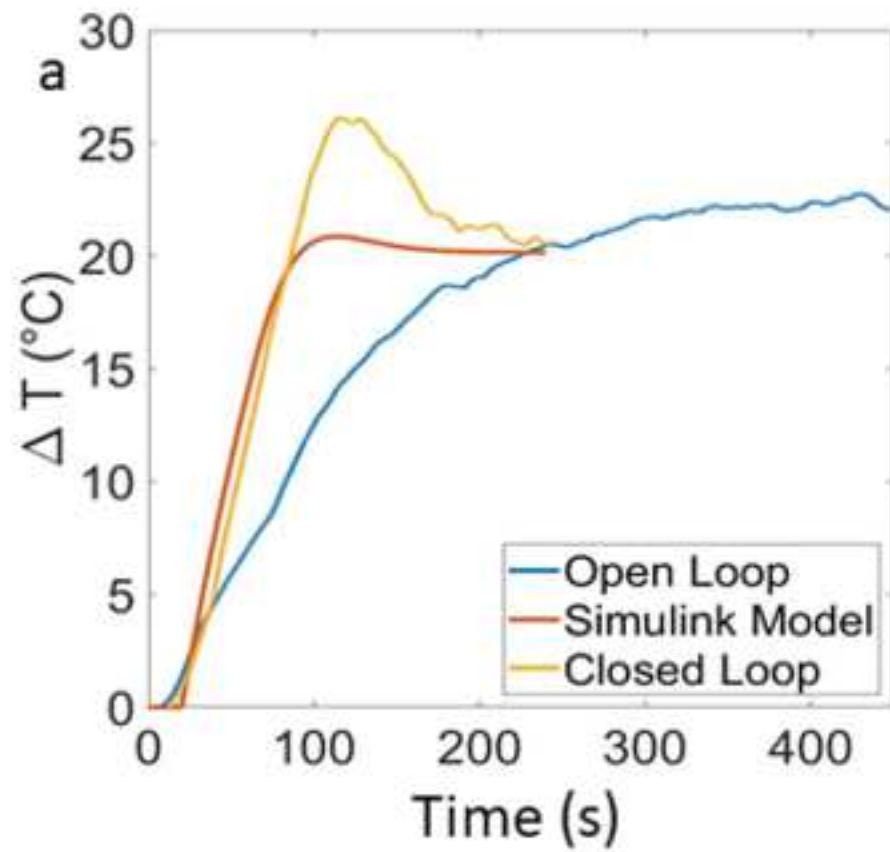


Figure 5

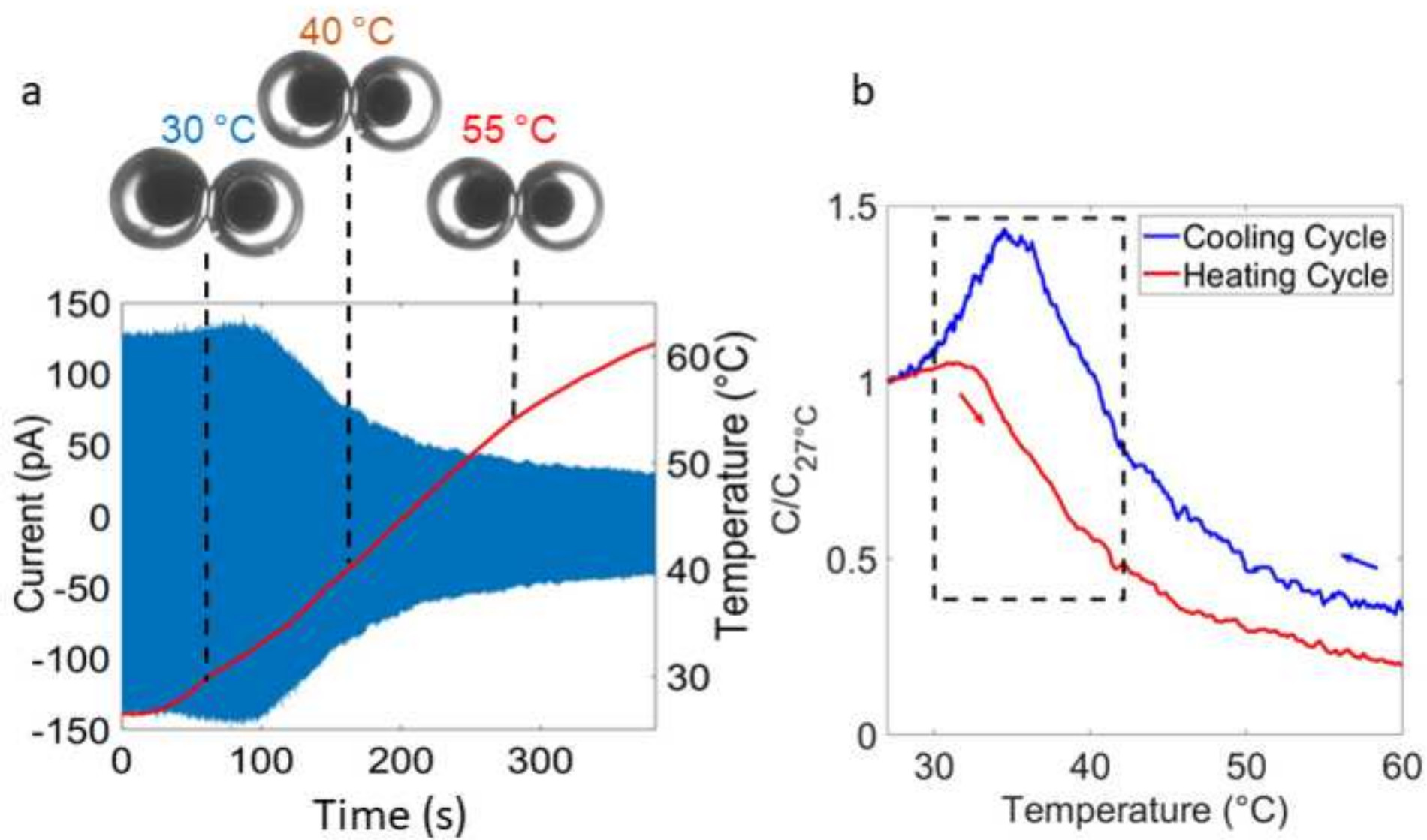


Figure 6

[Click here to access/download;Figure;Figure 6.png](#)

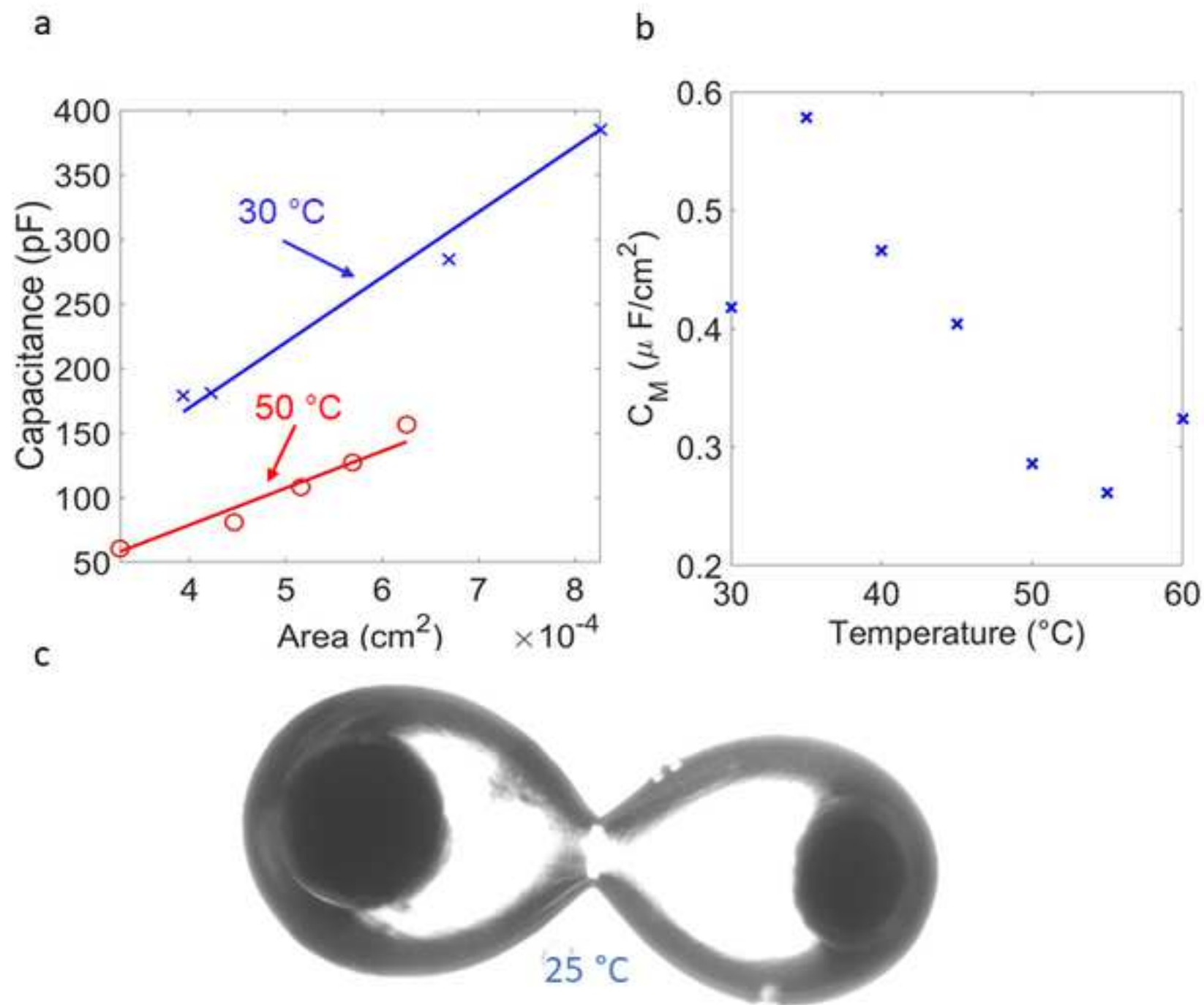
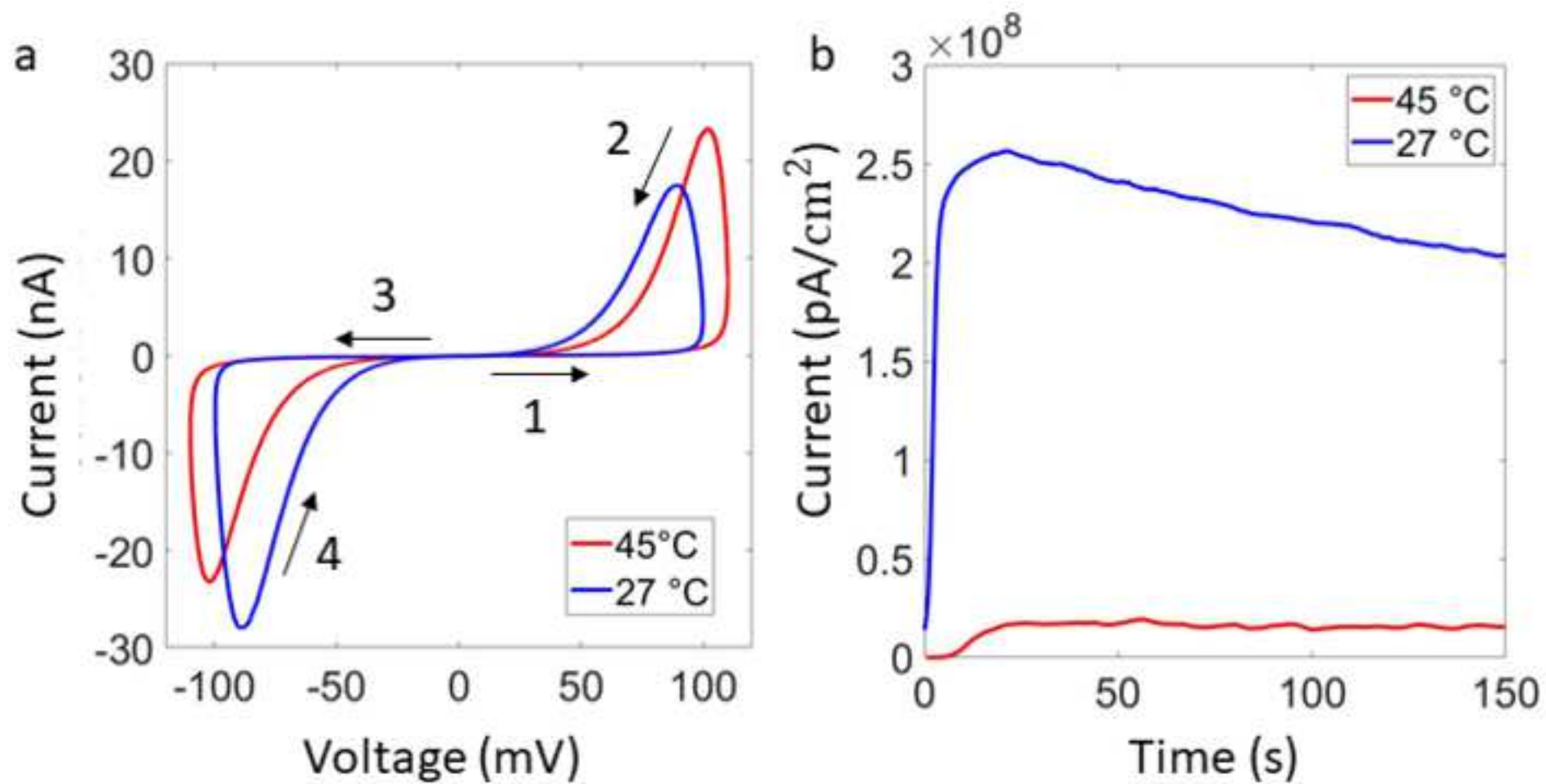


Figure 7



Name of Material/ Equipment	Company	Catalog Number	Comments/Description
25 mm x 25 mm x 1 mm insulative rubber (x2)	Any		Insulates the bottom of the aluminum fixture from the stage of the microscope
25 mm x 25 mm x 6 mm insulative rubber (x2)	Any		Protects heating elements from being damaged by the microscope stage clips and insulates the top of the heating elements.
3-(N-morpholino) propanesulfonic acid	Sigma Aldrich	M3183	Buffering agent for lipid solution
Acrylic substrate	Fabricated in house	HTD_STG_2	~1000 uL acrylic well with a poka-yoke exterior profile to fix orientation
Aluminum fixture	Fabricated in house	HTD_STG_1	Base fixture with an oil well that holds the acrylic fixture and includes two flat pads adjacent to the oil well for the heating elements
Brain Total Lipid Extract	Avanti	131101C-100mg	25 mg/mL porcine lipid extract
Compact DAQ Chassis (cDAQ)	National Instruments	cDAQ-9174	Chassis to house multiple types of sensor measurement or output modules
Data Acquisition System (DAQ)	Molecular Devices	Digidata 1440A	High resolution analog to digital converter
Fixed gain amplifier/power supply	Hewlett Packard	HP 6826A	Amplifies DC voltage output from the voltage output module
Heating element (x2)	Omega	KHLV-101/5	25 mm x 25 mm polyimide film kapton heating element with a 5 watt power limit.
M3 Stainless Steel Screw	McMaster Carr	90116A150	Secures thermocouple to aluminum fixture
Patch clamp amplifier	Molecular Devices	AxoPatch 200B	Measures current and outputs voltage to the headstage
Personal computer	Any		Computer with multiple high speed usb ports and a minimum of 6 Gb of ram
Potassium Chloride	Sigma Aldrich	P3911	Electrolyte solution of dissociated ions
Temperature input module	National Instruments	NI 9211	Enables open and cold junction thermocouple measurements for the cDAQ chassis
Thermocouple	Omega	JMTSS-020U-6	U-type thermocouple with a diameter of 0.02 inches and 6 inches in length

Voltage output module

National Instruments

NI 9263

Analog voltage output module for use with the  
cDAQ chassis

Waveform generator

Agilent

33210A

Used to output a 10 mV 10 Hz sinusoidal  
waveform

All editorial concerns have been addressed in the updated manuscript, figures, table of materials, and supplemental information. We greatly appreciate the editor's diligence in helping us to create the perfect manuscript to submit to JoVE.



We would like to extend a sincere thank you to each reviewer for evaluating our manuscript. We have itemized and addressed the feedback in the blue text below.

### Reviewer #1:

#### Minor Concerns:

1) The authors emphasize that the temperature control has two advantages: facilitating the DIB formation especially for lipids whose transition temperature is above room temperature and enabling temperature dependent experiments. The latter advantage is well illustrated by the representative results, but the former point may be more demonstrated. Could the authors provide an example of DIB formation which is very difficult at room temperature and made easier by the temperature raise induced by their setup?

Lipids with acyl chain melting points above RT require heating to achieve tightly-packed monolayers at the water-oil interface necessary for DIB formation. Examples include synthetic lipids such as di-palmitoyl phosphatidylcholine (DPPC), as well as natural cellular extracts, such as brain total lipid extract (BTLE) or *E. coli total* lipid extract (ETLE).

#### Changes to manuscript (lines 66-76)

*The majority of published experiments on model membranes, including those with DIBs, have been performed at room temperature (RT, ~20-25 C) and with a handful of synthetic lipids (e.g. DOPC, DPhPC, etc.). This practice limits the scope of biophysical questions that can be studied in model membranes and based on observation, it can also restrict the types of lipids that can be used to assemble DIBs. For example, synthetic lipids such as DPPC, which has a melting temperature of 42 °C, does not assemble tightly-packed monolayers or form DIBs at RT<sup>1</sup>. DIB formation at room temperature has also proven difficult for natural extracts, such as those from mammals (e.g. brain total lipid extract, BTLE)<sup>2</sup> or bacteria (e.g. Escherichia coli total lipid extract, ETLE)<sup>1</sup>, which contain many different types of lipids and originate from cells that reside at elevated temperatures (37 °C). Enabling study of diverse compositions thus provides opportunities to understand membrane-mediated processes in biologically relevant conditions.*

2) The hysteresis effect shown on figure 5b suggests that it is not equilibrium capacitance which is displayed. This should be commented maybe with a few words about the kinetics of the phenomena and experiment.

The data shown in figure 5b was normalized by the capacitance at 27 C and the hysteresis shown is due to irreversible changes in membrane area due to temperature changes in the oil bath.

### Changes to manuscript (lines 549-553):

*At this temperature, changes in acyl chain ordering in the membrane alter the solubility of oil in the core of the bilayer, which affects membrane thickness. Also, note that the hysteresis shown between the heating cycle and the cooling cycle is due to irreversible changes in bilayer area that occur between subsequent cycles, which were typically performed 10 min apart.*

3) To my opinion figure 6c is not sufficiently explained, I do not understand the graph.

We agree that Figure 6c is confusing. Our intention was to show the high adhesiveness of a BTLE bilayer when cooled below the lipid's melting temperature. The plotted data is a graph of capacitive current versus time, where the amplitude is proportional to the area of the membrane. The fact that the amplitude is steady shows the inability to change the bilayer area by moving the droplets, which hinders the experimenter from collecting specific capacitance data.

### Changes to figure:

*We have removed the plot of current versus time from Figure 6C.*

4) The ionophore Mz is not defined. A few words of explanation would be welcome.

Monazomycin (Mz) is a positively charged antibiotic that forms cation selective channels in lipid membranes<sup>3</sup>. Mz channels are comprised of six monomers<sup>4</sup> that are ~4 nm<sup>3</sup> in length. The monomers arrange themselves like staves in a wood barrel<sup>5</sup>, prior to insertion, and require a sufficient transmembrane voltage to insert and span the membrane.

### Changes to manuscript (pg 13)

*Monazomycin (Mz), a positively-charged antibiotic that forms cation selective channels through the bilayer at sufficient transmembrane potentials<sup>3</sup>, was chosen to demonstrate this relationship.*

5) The proposed method enables heating of the sample. Could it be easily extended to cooling by using Peltier devices?

Yes, a Peltier device could be integrated into the protocol if testing at temperatures below RT was of interest. However, other issues may arise. For instance, if the melting temperature was much lower than RT, the experimenter would have to choose an oil that would not freeze at lower temperatures, as hexadecane freezes at 18C.

## Changes to manuscript:

None required

### Reviewer #2:

We appreciate the reviewer's enthusiasm for our work. No changes requested.

### Reviewer #3:

Major points:

Abstract:

1) The abstract should start with one sentence addressing the advantages of the use of DIBs, for the audience who are not yet familiar with this.

We agree the advantages related to the DIB method should be introduced to the reader early to better explain the impact of the work described in the procedure. The DIB method is advantageous in that it allows for a tunable bilayer area, enables, asymmetric droplet and leaflet compositions, uses low droplet volumes, and can be easily scaled to larger droplet networks<sup>6</sup>. In addition, membranes formed in this way exhibit long lifetimes. This rationale has been included in the revised abstract.

### Change to manuscript (Abstract, lines 17-22):

The droplet interface bilayer (DIB) method for assembling lipid bilayers (i.e. 'DIBs') between lipid-decorated water droplets in oil offers key benefits versus other methods: DIBs are stable and often long-lasting, bilayer area can be reversibly tuned, leaflet asymmetry is readily controlled via droplet compositions, and tissue-like networks of bilayers can be obtained by adjoining many droplets. Forming a DIB requires spontaneous assembly of lipids into high density lipid monolayers at the surfaces of the droplets; this method is often employed at room temperature and with synthetic phospholipids, including those that happen to be in a liquid-disordered thermotropic phase.

2) The following sentence needs rephrasing: "These conditions yield well-packed monolayers and stable bilayers, but they also disguise the importance of temperature on lipid phase and assembly and bilayer structure." In order to not inadvertently disparage previous DIB work done at ambient temperature, it might be rephrased as: "These conditions yield well-packed monolayers and stable bilayers, but greater insight into importance of temperature on lipid phase and assembly and bilayer structure may be obtained by studies over varying temperatures."

Our goal here was to inform the reader that commonly used lipids (e.g. DPhPC) may not undergo thermotropic transitions and may differ substantially from some naturally occurring lipids. However, we appreciate your concern that our statement may be taken as a negative comment in regards to previous works that do not consider the effects of temperature. Thus, we have changed the manuscript per your recommendation.

#### **Change to manuscript (Abstract, lines 24-26)**

*These conditions yield well-packed monolayers and stable bilayers, but greater insight into importance of temperature on lipid phase and assembly and bilayer structure may be obtained by studies over varying temperatures.*

#### **Introduction:**

3) This section will benefit from greater background material on ion-channel kinetics, possibly in the final section of the introduction, to provide insight into the crucial components and concepts mentioned at the end of the results and conclusion sections.

The intent of this manuscript is to provide instruction for using feedback temperature control to prescribe the temperature of the oil bath and lipid solution used in DIB formation. Lines 80-89 in the original introduction section outlined effects that can be studied when temperature is varied, including identifying thermotropic transitions in lipids, quantifying changes in structure and transport properties of the membrane, and exploring the kinetics of membrane-active peptides and proteins at varying temperatures and across multiple membrane types. We had intended for this to provide the necessary background needed for a reader to understand the context of the results shown later in the manuscript.

Nonetheless, to further strengthen this connection, we revised the sentence in lines 87-90 and added new text at the end of the introduction to help the reader see the relationships between temperature, membrane properties/composition, and the kinetics of membrane active-species studies.

#### **Change to manuscript:**

(lines 89-92)

*... examine how lipid composition and fluidity affect the kinetics of membrane-active species (e.g. pore-forming peptides and transmembrane proteins<sup>1</sup>), including in mammalian and bacterial model membranes and at a physiological temperature (37 °C).*

(Lines 103-104)

*These techniques are important additions to the many biophysical studies that can be designed and performed effectively in DIBs, including studying the kinetics of membrane-active species in different membrane compositions.*

Protocol:

4) To enhance Figure 1, it would be helpful to have schematic views to show the involved steps, in addition to the top-down photos. The perspective of the photos makes it very difficult to perceive how the materials were layered/stacked on one another. There are no images or clarification as to what the acrylic reservoir is. Figure 1.7 does not clearly show what the latter looks like, or where it is placed. The main issue with the part of the protocol associated with "Figure 1", is the lack of detail regarding the construction of the aluminum fixture. This particularly becomes problematic when the protocol calls for adding oil to the system, since the location of where it is added is not clear.

Thank you for the suggestion.

#### **Change to manuscript:**

We have added an exploded view of the fixture and its components to the SI(S3).

5) Whenever the term "oil" is mentioned, does this mean the same chemical composition for oil (e.g., hexadecane), for both placement in the well of the aluminum fixture as well as between the walls of the acrylic reservoir and aluminum fixture? For example, please refer to Line 133: "Oil added to the viewing compartment of the aluminum fixture is used to match the refractive indices of the acrylic and glass for clearer imaging of the droplets contained within the acrylic reservoir." Would the use of different oils having different RI, influence the design of the set up, and are there any precaution that needs to be taken when using different oils?

There are several oil types that would match the RI close enough to enable imaging of the experiment, but clarification that hexadecane oil is being used in both the acrylic reservoir and the well of the aluminum fixture was lacking. Also, different oils could be used in each compartment, but we have not experimented with any potential combinations, nor have we seen reason to.

#### **Changes to manuscript (steps 1.8 and 1.9 of Protocol):**

*1.8. Dispense ~1000  $\mu$ L of hexadecane oil into the well of aluminum fixture (i.e. between the walls of the acrylic reservoir and aluminum fixture), taking care to not overfill. The oil level in the well of the aluminum fixture should be as high as allowable to provide a maximal surface area for heat transfer to occur, while not allowing oil to spill over the edges of the fixture onto the microscope stage or objective lens.*

1.9. *Dispense ~1000 uL of hexadecane oil into the acrylic reservoir, while remaining mindful to not overfill.*

6) Fig 2b image is blurry.

Figure 2b is clear in the original format. Perhaps there was an issue with the upload or the file conversion process.

### **Changes to manuscript:**

The figure was checked and uploaded again to try to fix any issues with image quality.

7) Protocol 2.3.5 (Lines 236-239) and Protocol 3.1 (Lines 261-262): More clarity is needed for both. It is recommended to split into two separate statements to avoid ambiguity.

On step 2.3.5, the added explanation of the role of the headstage took away from the clarity of the procedure step. This is better suited as a note below that procedure step to still provide the reader with relevant information about the function of the headstage. In regard to step 3.1, the first half of the procedure step is redundant information and does not add to the explanation of what should be accomplished on that step. Hence, it can be removed.

### **Changes to manuscript (steps 2.3.5 and 3.1 of the Protocol):**

*NOTE: The role of the headstage is to control the voltage between the electrodes and measure the resulting current, which is converted into a proportional voltage that gets output by the patch clamp amplifier to the DAQ-1.*

3.1. *Start the DAQ-2 software on the PC and open the temperature control VI file. Once the VI opens, open the VI again by clicking on the folder icon in the bottom left corner of the VI's GUI and selecting the temperature control VI.*

8) With regards to the open-loop, closed-loop temperature control responses and heating scenario systems and Simulink modeling: this section will be vague and obscure to anyone except those already familiar it. More explanation would be helpful.

Further explanation of open-loop and closed-loop heating have been added to the manuscript. We also have added references to outside resources in regard to Simulink and PI controllers<sup>7</sup>.

### **Changes to manuscript (section 3 of Protocol):**

*During open-loop heating, the prescribed heating power is independent of the measured temperature. In contrast, closed-loop heating consists of continually adjusting the applied power*

*to the heaters in a manner that helps drive the measured temperature closer to the desired temperature. This is achieved herein using a proportional-integral (PI) control scheme.*

9) At Line 314: "The formation of a tightly-packed interfacial bilayer, upon exclusion of excess oil, can be confirmed through visual inspection.": Hexadecane, the oil used in this particular protocol, is known to be substantially entrapped within the bilayer (10-30%). How then does one confirm "visually" that oil is completely excluded? Any visual images would be helpful to readers to show before and after exclusion of oil. What would be expected if a different oil (e.g., squalene) was used for this device?

The reviewer is correct; our original wording was misleading. Rather than viewing the exclusion of (all) excess oil, we meant to say that we are able to monitor changes in the appearance of the connected droplets upon thinning, a process that excludes some of the oil from between the two monolayers as they come together to form a bilayer. The visual changes that occur during DIB formation are well-documented<sup>8</sup>, therefore we chose not to show a before-and-after comparison. Rather, we included in Figure 5a images to show how temperature affects the appearance of a DIB at different temperatures. Separately, the reviewer asks an important question about the role of oil type on DIB formation and appearance. We have address this in a note corresponding to Step 3.8 as detailed below.

#### **Change to manuscript (step 3.8 of protocol):**

*The formation of a thinned interfacial bilayer can be confirmed through visual inspection (**Figure 5a**) or by measuring the increase in the amplitude of a square-waveform capacitive current induced by a waveform generator outputting a 10 mV, 10 Hz triangular voltage<sup>6</sup>.*

*NOTE: The type of oil can have a significant impact on bilayer thinning, membrane thickness, and inter-droplet contact angle. In general, the smaller the oil molecule the more easily it can remain in the hydrophobic core of the bilayer occupied by lipid acyl chains. Oil retention increases both monolayer and bilayer tensions and thickness and decreases the area and angle of contact between droplets. These metrics signify a weaker state of adhesion. Larger, bulkier molecules exert the opposite effect. For example, squalene is bulkier molecule than alkanes such as hexadecane, which enables it to be readily excluded from between monolayers during bilayer thinning. As such, DIBs formed in squalene are thinner, they display higher contact areas and angles, and they exhibit higher free energies of formation<sup>6,9</sup> (a measure of droplet-droplet adhesion).*

10) The paper focuses on a temperature-controlled study but the construction of the heating element /aluminum fixture, and information about the specifics of the heating element, is found only in the supplemental section. More detail on it should be placed in the main part of the paper.

We believe the addition of an exploded view in the SI, as mentioned in line item 4 of this response, will add clarity to the construction of the heated stage we propose.



Furthermore, the heated stage design we included is only one way of preparing a fixture to perform this task, as there have been other iterations of the fixture and other designs could be used in a similar manner to perform this experiment. The main purpose of the protocol is to teach the reader how to use a heated stage in conjunction with measurement equipment to identify and control the thermotropic phase behavior of membrane lipids, which is why these details were included in the SI.

#### **Change to manuscript:**

None.

11) Line 312, at point 3.7, it is recommended that the bilayer should equilibrate for at least 10 minutes to reach a steady interfacial area. Would the time depend on choice of lipid and/or of oil? If so, what is expected in terms of equilibration time? Also, upon bringing the electrodes together to form a bilayer, a recommendation is needed as to how to determine when to cease bringing them closer. Would this be simply at the point of first contact? It is likely that, even though the droplets may touch, a bilayer will not fully "zip" unless droplets are practically pushed together. There is a difficult balance between a contact being sufficient to form a bilayer, vs. a contact that does not (fully) form a bilayer, vs. a contact that precipitates droplet coalescence. These possibilities need to be clarified and explained (based on the author's experience), for the benefit of the non-experienced reader.

Lipid and oil types will definitely impact the time required to for tightly packed bilayer to form, but the best method to determine if the bilayer has reached an equilibrium state is to monitor the capacitive current<sup>6</sup> and visually inspect the bilayer area (Figure 5a). The droplets should be brought together until the user can see the droplets start to deform or displace each other. If a bilayer does not form after several minutes, the droplets can be forced together further, but this typically is not required. We have included this additional detail in Step 3.8.

#### **Change to manuscript (step 3.7 which is now step 3.8 of protocol):**

*3.8. Bring the droplets into gentle contact by slowly manipulating the horizontal positions of the electrodes until the user sees the droplets deform from contact or begin to displace on another and wait a few minutes until bilayer formation commences. If after several minutes a bilayer has not formed, the droplets can be coerced together more to facilitate bilayer formation.*

12) In bullet 4.2.1.2 (line 334) how does one measure bilayer area? How is an image captured of the bilayer? While this may have been already discussed elsewhere, however, it would useful to compile all the necessary steps for the readers, considering that this is a methods paper.

We appreciate the reviewer's suggestion. We have added text describing the use of a camera that captures images of the bilayer (as viewed from below) through the



objective of the microscope stage. This is a critical part of the process for determining specific capacitance of the membrane and the addition of this text will add value to the protocol. We utilize a custom Matlab script that calculates bilayer area from DIB images. This is achieved by identifying the edges of the droplets (i.e. intersecting circles), measuring the interfacial contact length, and then calculating area by using the contact length as the diameter of a circle or ellipse, as discussed elsewhere<sup>6</sup>.

#### **Change to manuscript (step 4.2.1.2 of the Protocol and NOTE added):**

*...collect images of the DIB to enable calculation of membrane area versus time by using a camera mounted to the microscope to image the bilayer as seen from the aperture of the microscope stage.*

*NOTE: As discussed elsewhere<sup>6</sup>, bilayer area is calculated from the contact length between droplets, which appear as overlapping circles in a bottom-view image. The positions and dimensions of the droplets, and the length of the contact line, can be calculated using an image-processing software or with other scientific programming tools.*

13) It would be helpful to see illustrate how capacitance is calculated from the current response. The average reader may not know how to do this. Same comments as above. Regardless whether this has been explained in different paper, it is still expected to be repeated here, at least in some fashion, for complete understanding without having to read separate papers to fill the gap.

We agree that a brief explanation of determining capacitance from the current response will be of value in this step. The square wave current response of a bilayer is proportional to its capacitance, as seen in the relationship<sup>10</sup>, and as such capacitance can be extracted from the amplitude of the square-wave current response.

#### **Change to manuscript:**

*NOTE: Nominal capacitance can be calculated from the amplitude of square-wave current<sup>10</sup>, using the relationship,  $C = \frac{I}{\omega V}$ , where  $C$  is equal to four times the product of amplitude ( $I$ ) and frequency ( $\omega$ ) of the applied triangular voltage. From these equations,  $C = \frac{I}{\omega V}$ .*

14) In step 4.2.1.2, there is discussion regarding the separation of the electrodes to modulate bilayer area: some explanation is needed as about how precise control of the electrodes can be achieved. I imagine ready rupture of the bilayers upon coarse movement of the electrodes.

Section 4.2.1.2 describes the method by which the droplets are mechanically manipulated, via micro-manipulators, to facilitate changes in bilayer area. Micro-manipulators allow for precise control of the electrodes and thus the contact between droplets, but coarse manipulation of the droplet will lead to a failed experiment by coalescence of the droplets or the droplet falling off the electrode.

### Change to manuscript (after protocol step 4.2.1.2):

NOTE: Micro-manipulators allow for precise control of the electrodes and thus gentle contact between droplets. Coarse manipulation of the droplets can lead to a failed experiment by coalescence of the droplets or by causing a droplet to fall off the electrode.

### Representative Results:

15) Line 529-530: It is stated that cooling the bilayer reverses the effects of increased temperature (thickened membrane, reducing contact area). It would be helpful to see the data showing a heated membrane being cooled over time. Is there hysteresis during heating and cooling?

This data for a membrane being cooled is provided in figure 5b and expanded upon in the specific capacitance plots in figure 6a. The temperature where the nonmonotonic change in capacitance occurs (figure 5b) is related to a change in bilayer thickness due to exclusion of oil from the membrane. Likewise, the change in slope of the specific capacitance plots in figure 6a also showcase the impact of a thickened membrane at lower temperatures.

### Change to manuscript (lines 547-458):

*The temperature where the nonmonotonic change in capacitance occurs corresponds to a change in bilayer thickness from exclusion of oil from the membrane<sup>2</sup>.*

### Discussion:

16) The need for a Faraday cage is mentioned in the discussion section. This should be included in the protocol.

We agree this detail should be included. The Faraday cage is crucial in eliminating outside noise from measurement of currents in the pA-nA range. Excessive noise from the environment can sequester small bilayer currents from the experimenter and should be at the forefront of the experimental procedure.

### Change to manuscript (added section 3.7 to protocol):

*3.7. Cover the headstage and heated stage fixture with a grounded Faraday cage.*

17) It has been discussed that the positions of the electrodes, and how resting on the

substrate, can distort the droplets' shape and complicate bilayer area calculations. It was recommended that the reader takes this into account. However, the manuscript does not provide any other information on how to image the bilayer or perform their image analysis to calculate area.

Imaging of the bilayer was addressed in line item 12 of response to the reviewers. However, an explanation of the area calculation was not included in the manuscript and the addition of explanation would benefit the text. This explanation was also addressed in item 12.

#### **Change to manuscript:**

Resolved in response 12.

18) It would be useful to include the monolayer equilibration time. If there are data already collected to determine optimal temperature and time for this process, then it would be useful to have such data. Even if some of data are disclosed elsewhere, it would be helpful for readers to see all relevant factors in this protocol.

In protocol step 3.6 we suggest a monolayer equilibration time of 10 minutes. Likewise, we proposed the use of interfacial tension measurements to assess monolayer formation and differential scanning calorimetry to measure critical transition temperatures, thinking these techniques would aid the reader in choosing conditions conducive to monolayer assembly. However, the “time” required for the equilibration was not explicitly discussed. Thus, we updated this discussion to indicate that critical time and temperature info can be gained via these complementary approaches.

#### **Change to manuscript: (lines 695-711)**

*For a previously untested lipid composition, key unknowns are the incubation time and temperature required to enable sufficient monolayer assembly at the surfaces of the droplets. The general rule is to heat the oil to a temperature above , where lipid mobility is enhanced allowing for faster lateral diffusion and tighter packing at the oil-water interface<sup>11</sup>, and wait long enough such that monolayer packing at the oil-water interface is high. The user may review published literature or consider their own complementary measurements to determine suitable time and temperature values: interfacial tension measurements on a pendant drop goniometer can be used to assess the time required for monolayer assembly<sup>12</sup> and differential scanning calorimetry is often used to identify thermotropic transitions of lipids<sup>2</sup>. Or an iterative approach may be pursued to identify suitable time and temperature where bilayer formation is consistent, the membrane is stable for more than a few minutes, and the resistance of the bilayer is >1 G. In recent studies with *E. coli* total lipid extract (ETLE)<sup>1</sup> and BTLE<sup>2,13</sup> a starting temperature >50 °C consistently leads to stable bilayer formation. Similarly, the minimum stable temperature after DIB for a given lipid type may also vary between lipid selections. For example ETLE DIBs can be cooled to 25 °C<sup>14</sup>, whereas single component DPPC DIBs*

*always coalesced below ~40 °C<sup>2</sup>. Observation has shown that BTLE DIBS show that 27 °C is a safe minimum temperature for maintaining a stable bilayer.*

Minor points:

Reference:

19)#39 and #41 are the exactly the same except for the publication year; one of these references is thus wrong and the other is redundant.

Thank you for catching this mistake. We have corrected the error in the references.

**Change to manuscript:**

*Removed erroneous reference and fixed the in-text citation.*

Table of Materials section:

20) Acrylic substrate and aluminum fixture have a catalog number provided but no company specified.

These pieces are to be fabricated by the experimenter and cannot be purchased off-the-shelf, and as such we have provided the necessary blueprints if they wish to follow our design. Because of this, no manufacturer was listed in the table of contents.

**Change to table:**

*“Fabricated in-house” was added under the company heading.*

21) Potassium chloride is listed but not mentioned anywhere else in the document.

Potassium chloride or sodium chloride are essential components of electrophysiology experiments and the reader is referenced to a previous JoVE protocol published by our lab for these details<sup>15</sup>. We have included this definition. Separately, during investigation of this line item we discovered that we had another duplicate reference in the text which needs to be removed.

Changes to manuscript:

3.6. Pipette a 250 nL droplet of aqueous lipid solution containing 2 of BTLE, 100 mM potassium chloride (KCl), and 10 mM 3-(N-morpholino) propanesulfonic acid (MOPS) onto each ...

- 1 Taylor, G. J. Sarles, S. A. Heating-Enabled Formation of Droplet Interface Bilayers Using Escherichia coli Total Lipid Extract. *Langmuir*. **31** (1), 325-337, (2015).
- 2 Taylor, G. J. *et al.* Capacitive Detection of Low-Enthalpy, Higher-Order Phase Transitions in Synthetic and Natural Composition Lipid Membranes. *Langmuir*. **33** (38), 10016-10026, (2017).
- 3 Muller, R. U. Peskin, C. S. The kinetics of monazomycin-induced voltage-dependent conductance. II. Theory and a demonstration of a form of memory. *The Journal of general physiology*. **78** (2), 201-229, (1981).
- 4 Muller, R. U. Finkelstein, A. Voltage-dependent conductance induced in thin lipid membranes by monazomycin. *The Journal of general physiology*. **60** (3), 263-284, (1972).
- 5 Andersen, O. S. Muller, R. U. Monazomycin-induced single channels. I. Characterization of the elementary conductance events. *The Journal of general physiology*. **80** (3), 403-426, (1982).
- 6 Taylor, G. J., Venkatesan, G. A., Collier, C. P. Sarles, S. A. Direct in situ measurement of specific capacitance, monolayer tension, and bilayer tension in a droplet interface bilayer. *Soft Matter*. **11** (38), 7592-7605, (2015).
- 7 Wang, Y.-G. Shao, H.-H. Optimal tuning for PI controller. *Automatica*. **36** (1), 147-152, (2000).
- 8 Dixit, S. S., Pincus, A., Guo, B. Faris, G. W. Droplet shape analysis and permeability studies in droplet lipid bilayers. *Langmuir : the ACS journal of surfaces and colloids*. **28** (19), 7442-7451, (2012).
- 9 Needham, D. Haydon, D. A. Tensions and free energies of formation of "solventless" lipid bilayers. Measurement of high contact angles. *Biophysical journal*. **41** (3), 251-257, (1983).
- 10 Sarles, A. *Physical Encapsulation of Interface Bilayers*, (2010).
- 11 Nenninger, A. *et al.* Independent mobility of proteins and lipids in the plasma membrane of Escherichia coli. *Molecular microbiology*. **92** (5), 1142-1153, (2014).
- 12 Venkatesan, G. A. *et al.* Adsorption Kinetics Dictate Monolayer Self-Assembly for Both Lipid-In and Lipid-Out Approaches to Droplet Interface Bilayer Formation. *Langmuir*. **31** (47), 12883-12893, (2015).
- 13 Najem, J. S. *et al.* Memristive Ion Channel-Doped Biomembranes as Synaptic Mimics. *ACS Nano*. **12** (5), 4702-4711, (2018).
- 14 Taylor, G. J. Sarles, S. A. Heating-enabled formation of droplet interface bilayers using Escherichia coli total lipid extract. *Langmuir*. **31** (1), 325-337, (2014).
- 15 Au - Najem, J. S. *et al.* Assembly and Characterization of Biomolecular Memristors Consisting of Ion Channel-doped Lipid Membranes. *JoVE*. doi:10.3791/58998 (145), e58998, (2019).

## Supplemental Information

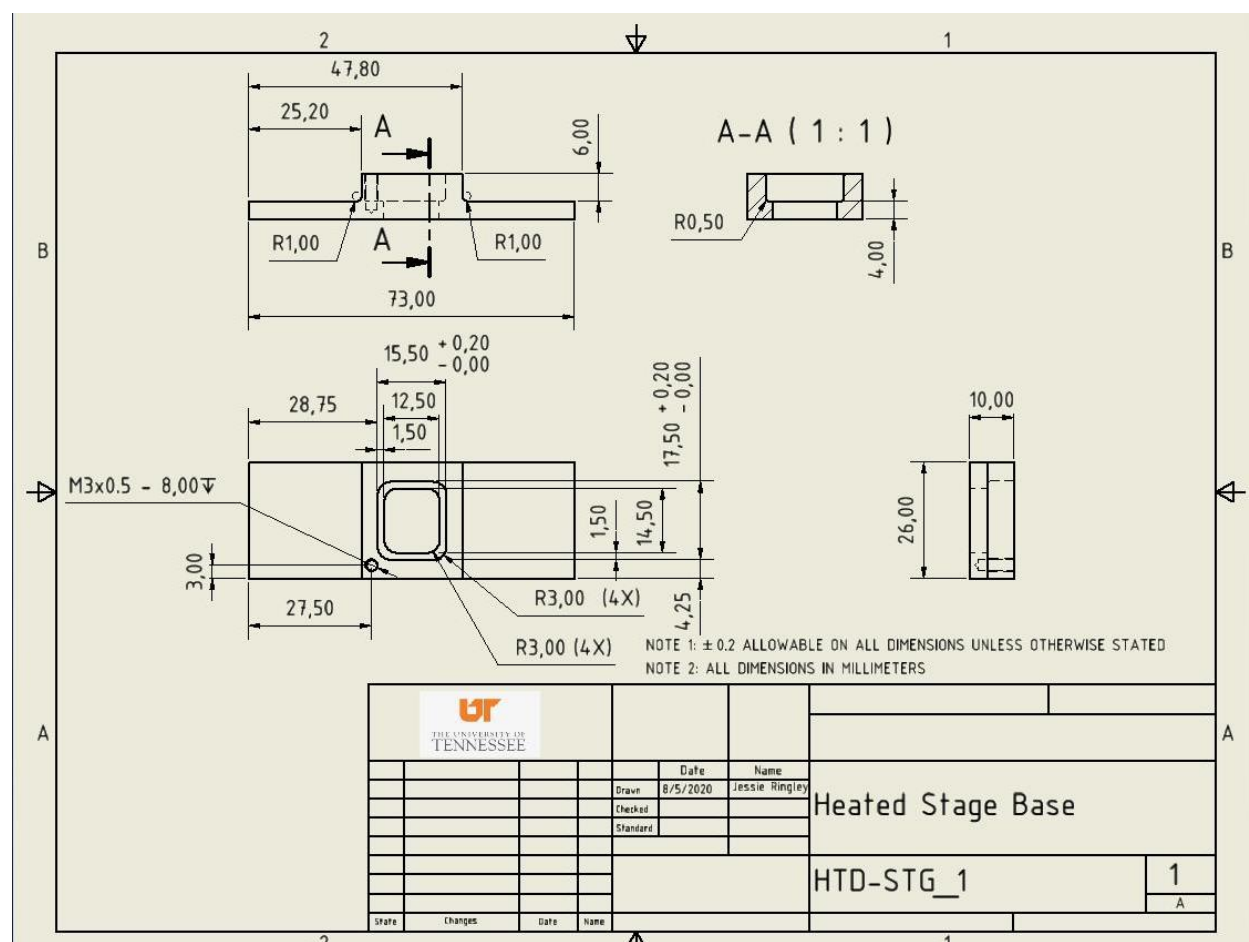


**Figure S1: Aluminum Fixture** This drawing shows the necessary dimensions and features for fabrication of the aluminum fixture that is the base of the heated stage. The 25.2 mm X 26 mm flat spots adjacent to the oil well were designed to allow for a maximal amount of surface-area contact between the fixture and the heating elements for heat conduction. Likewise, aluminum was chosen for the base fixture material due to its high thermal conductivity. The M3 X 0.5 mm screw hole called out in the print is used to secure and position the thermocouple in the oil well.

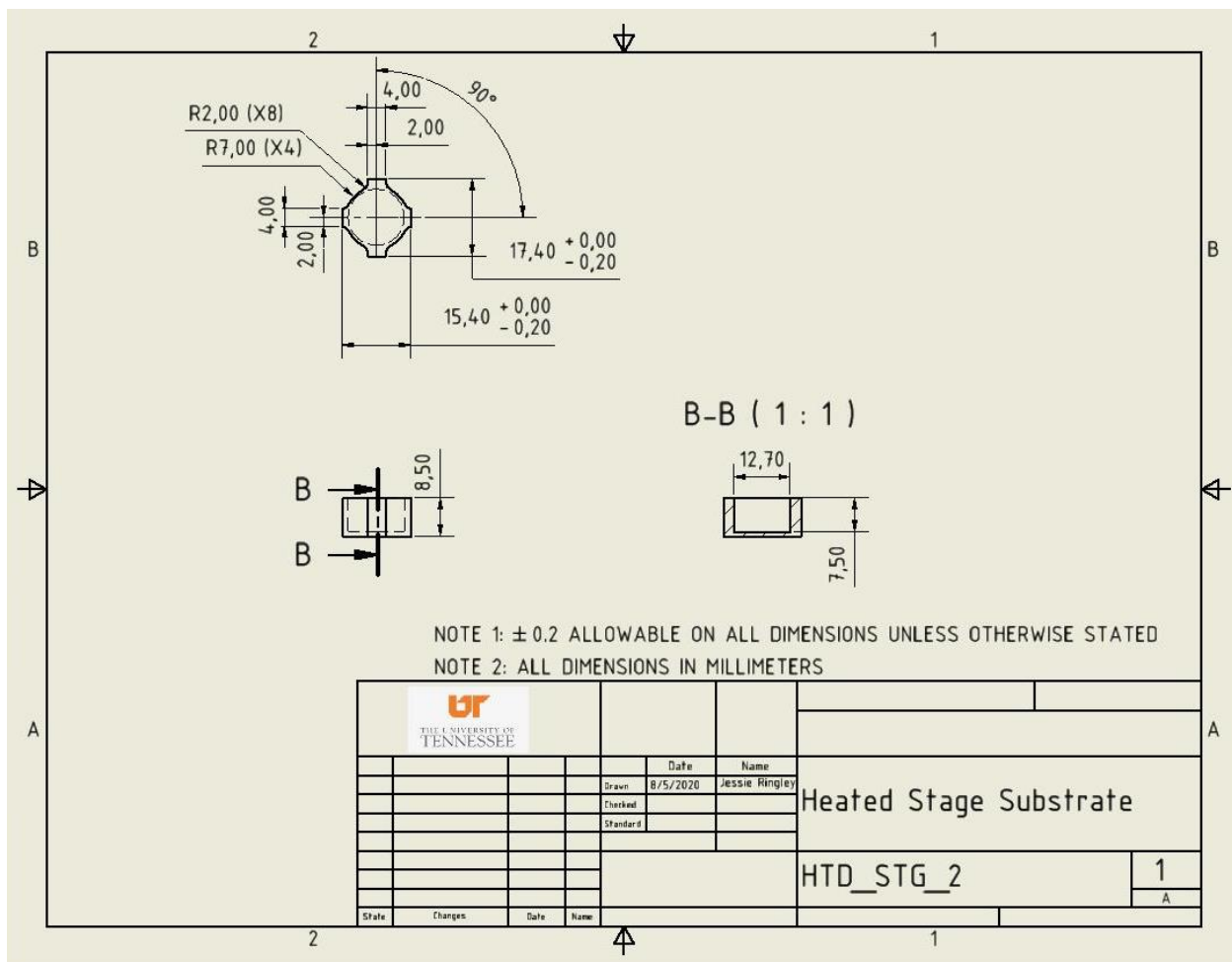


**Figure S2: Acrylic Substrate** The acrylic substrate is relatively simple piece to fabricate, with no critical outstanding features, except for the profile. The exterior profile was designed with Poka-yoke in mind so the acrylic substrate can only be oriented in the fixture in such a way to allow ample room for the thermocouple to fit in the oil well.



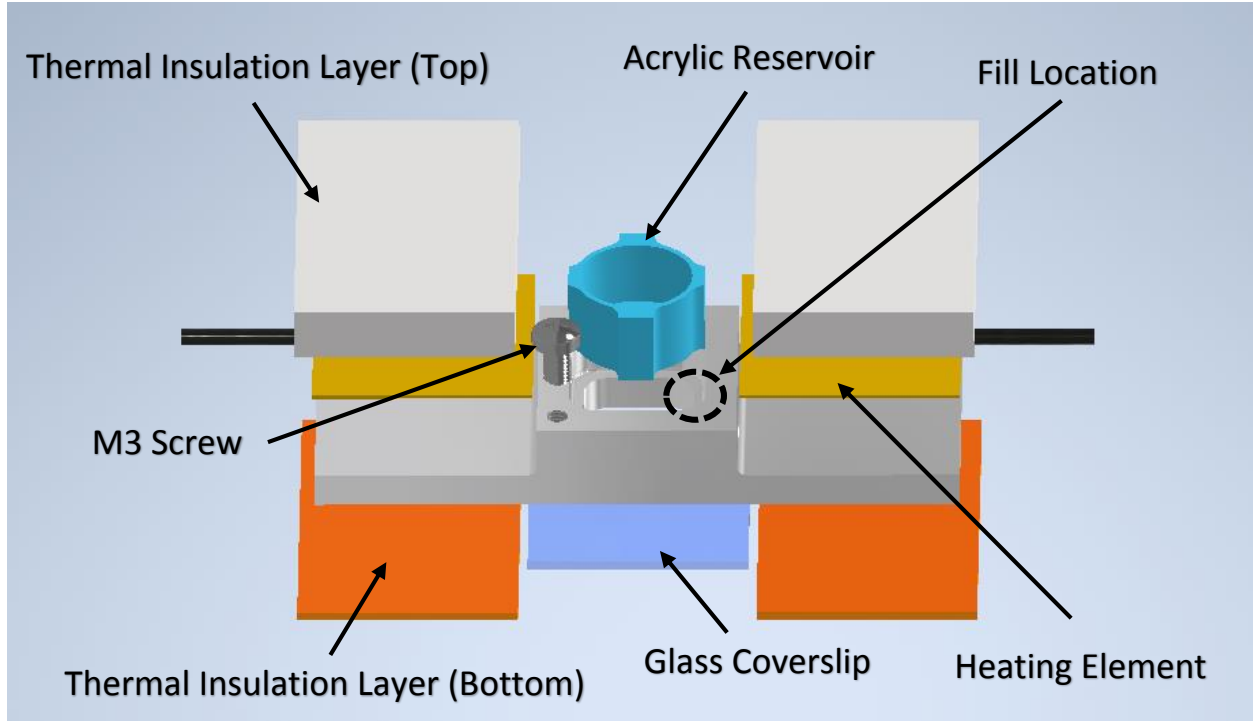


**Figure S3: Acrylic Substrate** An exploded view of the assembled-heated stage has been provided to aid the experimenter during initial setup. Also, take note of the area highlighted by the dashed circle, as this is the ideal position to fill the aluminum fixture with oil during protocol step 1.8.

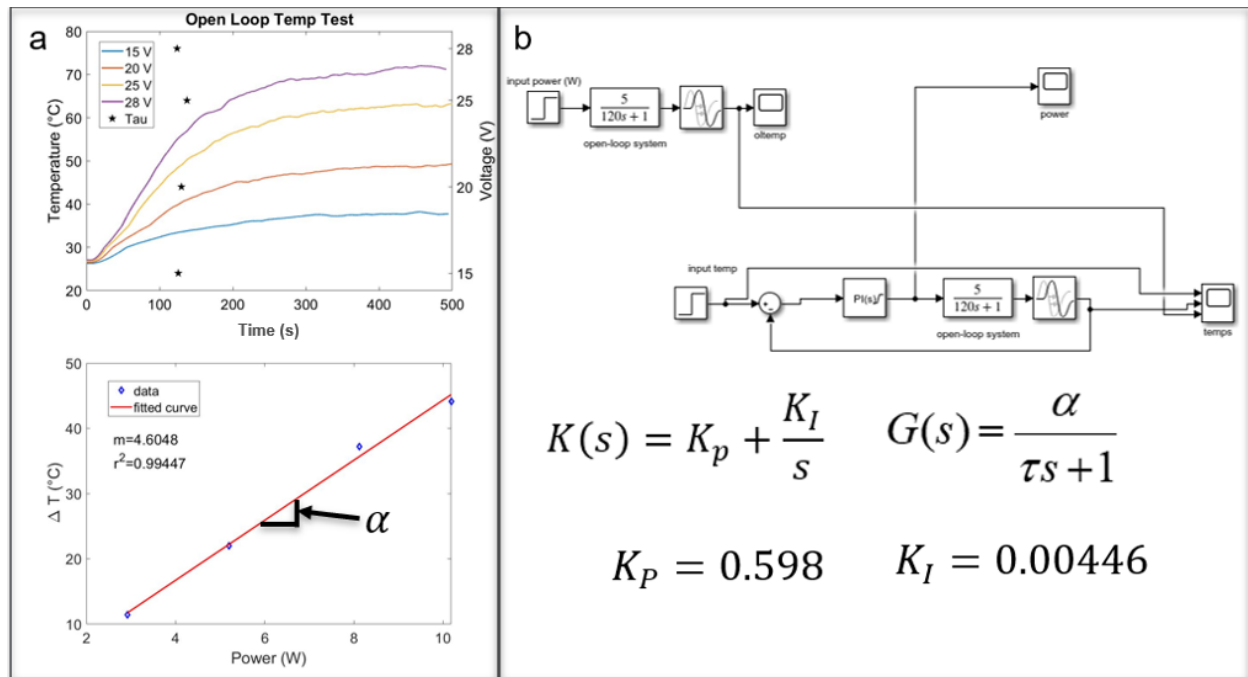


**Figure S4: Open Loop Data and Simulink Modeling** Panel (a) shows the open-loop temperature responses to varying dc power levels that were used to assess the delay time,  $t_d$ , the time constant,  $\tau$ , and open-loop heating gain,  $\alpha$ , of the system. The delay time represents the time lag



before temperature starts rising ( $\sim 20$  s). Each value of  $\tau$  (marked by \*,  $\sim 125$  s) is defined as the time required for 63.2% of the total rise in temperature to occur. Panel (b) shows the steady-state change in temperature ( $\Delta T$ ) versus the applied power. The slope of the data plotted in (b) was used to compute the  $\alpha$ , which represents the ratio of temperature change per supplied power. These parameters were used in the Simulink model shown in panel (c) and provided as a supplementary file to tune the PI controller to achieve a desired closed-loop temperature control response.

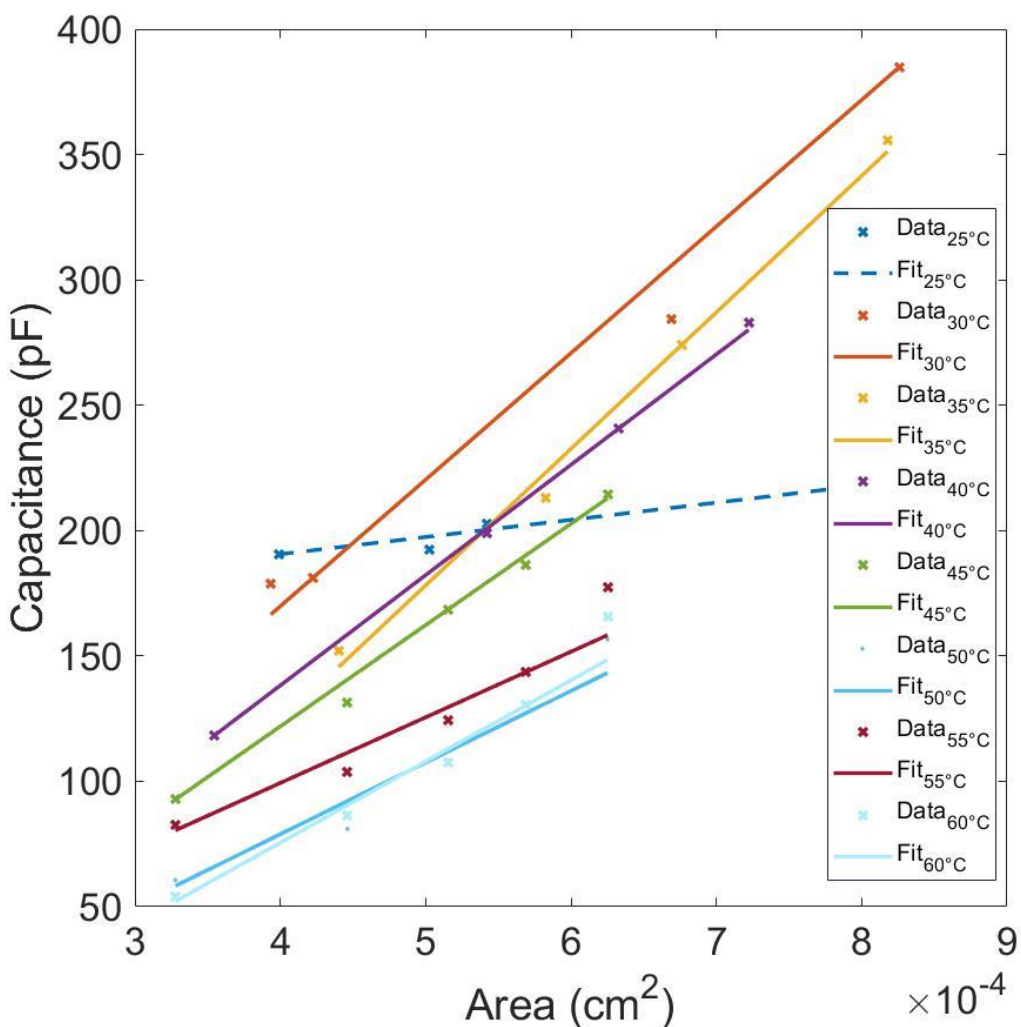
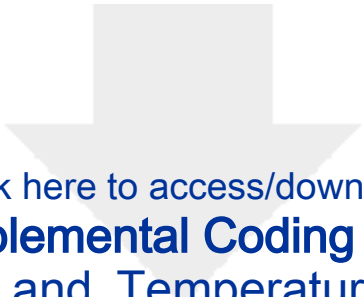
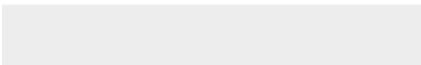



**Figure S5: Additional Specific Capacitance Data** The plots shown in **Figure 6a** and **6b** were compiled from this specific-capacitance ( $C_M$ ) data set. This plot also showcases the inability to accurately measure capacitance at temperatures of 25 °C and below, therefore this measurement was excluded from the dataset. The area changes necessary for an accurate  $C_M$  measurement require excessive force to be applied to the droplets from the micro-manipulators, which causes severe distortion of the droplets shape and area of contact.





Click here to access/download  
**Supplemental Coding Files**  
DC\_Steps\_and\_TemperatureControl.vi



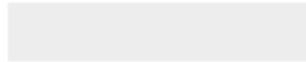


Click here to access/download  
**Supplemental Coding Files**  
PID\_GT\_subVI.vi



[Click here to access/download](#)

**Supplemental Coding Files**  
**TempControlENUMtypedef.ctl**





[Click here to access/download](#)

**Supplemental Coding Files**

DAQmx4\_thermocouple\_channels(2).vi






[Click here to access/download](#)

## **Supplemental Coding Files**

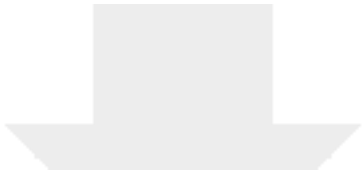
DAQmx\_AnalogOut\_100k\_fourchannels.vi





[Click here to access/download](#)  
**Supplemental Coding Files**  
CumError.vi





Click here to access/download  
**Supplemental Coding Files**  
tempPID2.slx

